iScience

CellPress
OPEN ACCESS

Perspective

Prospect of Spin-Orbitronic Devices and Their Applications

Yi Cao,[1,4] Guozhong Xing,[2,4] Huai Lin,[2] Nan Zhang,[3] Houzhi Zheng,[3] and Kaiyou Wang[1,3,*]

SUMMARY

Science, engineering, and medicine ultimately demand fast information processing with ultra-low power consumption. The recently developed spin-orbit torque (SOT)-induced magnetization switching paradigm has been fueling opportunities for spin-orbitronic devices, i.e., enabling SOT memory and logic devices at sub-nano second and sub-picojoule regimes. Importantly, spin-orbitronic devices are intrinsic of nonvolatility, anti-radiation, unlimited endurance, excellent stability, and CMOS compatibility, toward emerging applications, e.g., processing in-memory, neuromorphic computing, probabilistic computing, and 3D magnetic random access memory. Nevertheless, the cutting-edge SOT-based devices and application remain at a premature stage owing to the lack of scalable methodology on the field-free SOT switching. Moreover, spin-orbitronics poises as an interdisciplinary field to be driven by goals of both fundamental discoveries and application innovations, to open fascinating new paths for basic research and new line of technologies. In this perspective, the specific challenges and opportunities are summarized to exert momentum on both research and eventual applications of spin-orbitronic devices.

INTRODUCTION

The advancement of new communication technologies prompts the society functions into the surge of the information era. Energy-efficient and intelligent information processing is one of the keystone research fields in science, engineering, and medicine arena. For more than half a century, the ferromagnets (FMs) have been used to store information since the advent of magnetic hard disk drive. Practically, the magnetic information stored in the form of magnetic orientations has to be presented and manipulated in an electrical way before its applicable implementation. Early magnetic information was written and read by the Oersted field and the induction electromotive force generated via solenoid coils, respectively, which was inferior in energy efficiency and device scalability. Thanks to the advance of nanotechnologies, on the one hand, the reading issues were resolved by using more efficient magnetoresistance-type read head based on the specific revolutionary effect of anisotropy magnetoresistance (AMR), giant magnetoresistance (GMR), and tunneling magnetoresistance (TMR), which opened up the research area of spintronics (McGuire and Potter, 1975; Baibich et al., 1988; Binasch et al., 1989; Djayaprawira et al., 2005). On the other hand, in addition to the electrical detection of magnetization, the experimental realization of current-driven magnetization switching by spin-transfer torque (STT) in a magnetic tunnel junction (MTJ, i.e., an FM/barrier/FM structure, such as CoFeB/MgO/CoFeB, the resistance that depends on the relative magnetic orientation of the two FMs) has fueled intensive interests in spintronic community since 1996 (Berger, 2008; Slonczewski, 1996; Brataas et al., 2012). Taking the merits of TMR reading and STT writing of the perpendicular magnetic anisotropy (PMA) FM free layer in an MTJ, the scalable commercial perpendicular MTJ-based STT-magnetic random access memory (MRAM) was successfully produced by Everspin Technologies in August 2016 (Slaughter et al., 2016) and pilot production was further started on 28-nm 1-Gb STT-MRAM chips in June 2019 (Aggarwal et al., 2019). The STT configuration is schematically shown in Figure 1A, where a spin-polarized electrons flux is generated owing to the interaction of electron spins and the magnetization when the current passes through (or is reflected by) the FM reference layer, and thereby transfers spin angular momentum to the local magnetization $\boldsymbol{M}$ of the FM free layer via tunneling barrier layer. This spin angular momentum gives an additional torque $\boldsymbol{\tau_{STT}}$ acting on the precessional magnetization dynamics expressed by the Landau-Lifshitz-Gilbert-Slonczewski (LLGS) equation (Slonczewski, 1996; Brataas et al., 2012):

[1]Beijing Academy of Quantum Information Sciences, Beijing 100193, P. R. China

[2]Key Laboratory of Microelectronic Devices & Integrated Technology, Institute of Microelectronics, Chinese Academy of Sciences, Beijing 100029, P. R. China

[3]State Key Laboratory of Superlattices and Microstructures, Institute of Semiconductors, Chinese Academy of Sciences, Beijing 100083, P. R. China

[4]These authors contributed equally

*Correspondence: kywang@semi.ac.cn

https://doi.org/10.1016/j.isci.2020.101614

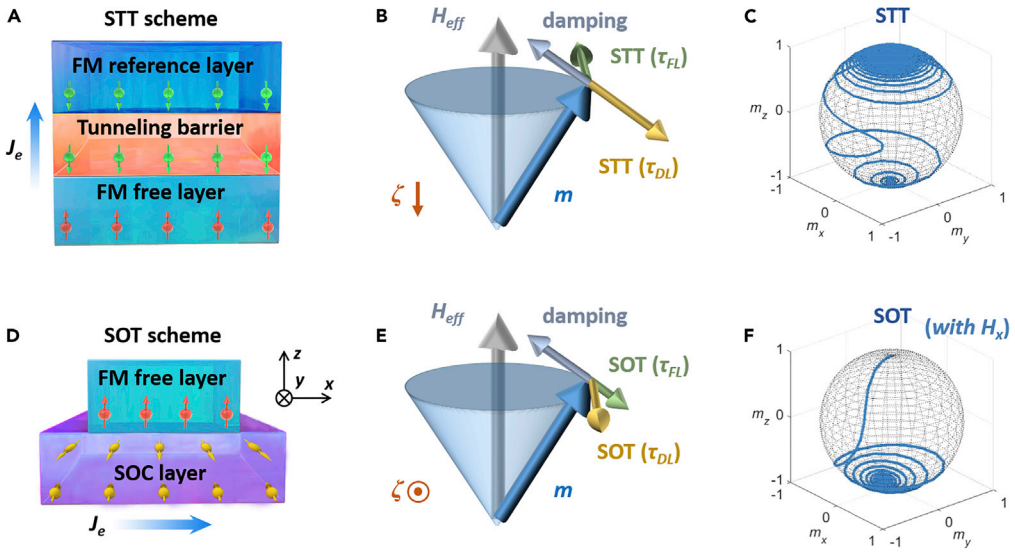

Figure 1. Comparisons between STT and SOT Schemes

Schematic (A–C) STT and (D–F) SOT-associated device configuration, damping and damping-like torque under effective magnetic field, and corresponding precession dynamic trajectories. Note that the damping-like SOT only drives the magnetic moment ***m*** toward an in-plane direction, hence an orthogonal external in-plane magnetic field H_x is generally required to break the symmetry and results in a deterministic SOT-induced magnetization switching.

$$\frac{dM}{dt} = -\gamma M \times H_{eff} + \frac{\alpha}{M_s}\left(M \times \frac{dM}{dt}\right) + \frac{\gamma}{\mu_0 M_s}\boldsymbol{\tau}_{STT}, \qquad \text{(Equation 1)}$$

where γ is the gyromagnetic ratio; H_{eff} is the effective magnetic field determined by the external field, the anisotropy field, and the exchange fields; α is the Gilbert damping constant; and M_s is the saturation magnetization of the FM free layer. Before the STT-induced switching, a sufficient thermal fluctuation is necessarily required, which deflects the magnetic moment from the static direction (e.g., the ***z***-direction for a PMA type STT) with a small angle. As depicted in Figure 1B, the damping-like term of $\boldsymbol{\tau}_{STT}$ counter-interacts reversely to the damping torque that tends to align the magnetization toward the effective field direction, resulting in gradually widened precession radius before the magnetic moment finally switches to the other magnetization orientation. This results in a dilemma over the energy efficiency of STT-induced magnetization switching because the switching speed tends to be slow (about 1–10 ns, due to incubation precession as illustrated in Figure 1C) under a moderate current density; in contrast, a faster switching with less precession circles requires much larger current density (Kiselev et al., 2003). Furthermore, STT-MRAM suffers from the endurance issue since the ultra-thin tunneling barrier layer (typically 1–2 nm) between two FM layers is required to transmit large writing current at a high frequency.

Over the last decade, the experimental observation and progress of spin-orbit torques (SOTs) (Miron et al., 2011; Liu et al., 2012) induced magnetization switching has elaborated its potential to overcome the aforementioned technical hurdles that STT is encountering. Both the spin current generation and the magnetization switching mechanism of SOTs are different from the counterpart of STT scheme. Specifically, the generation of SOTs is originated from the fundamental spin-orbit coupling (SOC), a relativistic interaction of a moving particle with momentum ***p*** and spin vector $\boldsymbol{\sigma}$ in an electric field E potential. The Zeeman energy of the SOC can be expressed as (Manchon et al., 2015)

$$\widehat{H}_{SO} \sim \mu_B(E \times p)\cdot\boldsymbol{\sigma} \Big/ mc^2, \qquad \text{(Equation 2)}$$

where μ_B, m, and c are the Bohr magneton, the particle mass, and the speed of light, respectively. Depending on the origin of E, two main types of SOC effects have been observed in the solid state, i.e., the Dresselhaus SOC with E originates from the bulk inversion asymmetry (BIA) such as the asymmetry in crystal structures or strain induced deformations, whereas the Rashba SOC with E stems from the structural inversion asymmetry (SIA) such as the lack of spatial inversion symmetry at the interfaces or surfaces. Both Dresselhaus and Rashba SOCs lock the spin to the momentum, and the spin-momentum locking

converts an in-plane charge current to a spin accumulation with non-equilibrium density at the surface or interface. Considering the Rashba SOC, the accumulated spin density is given by (Manchon et al., 2015)

$$\boldsymbol{S} = \alpha_R m(\boldsymbol{z} \times \boldsymbol{j}_e)/e\hbar, \quad \text{(Equation 3)}$$

where α_R is the Rashba parameter, $\boldsymbol{z}$ is the out-of-plane unit vector, $\boldsymbol{j}_e$ is the charge current density, and $\hbar$ is the reduced Planck's constant, which is known as the Rashba-Edelstein effect (or the Edelstein effect, sometimes also called the inverse spin galvanic effect, iSGE, which describes the generation of a nonequilibrium spin density by a charge current) (Edelstein, 1990). Another typical scheme of charge-to-spin conversion the resulted from SOC is the spin Hall effect (SHE), a transport phenomenon that depicts that a charge current generates transverse spin currents and the spin polarization vectors of which are orthogonal to both charge and spin current directions. The SHE is ascribed to two plausible mechanisms, namely, the extrinsic (electrons scattering against spin-orbit coupled impurities, i.e., Mott scattering) and/or the electron trajectories deflection driven by the intrinsic SOC (Berry phase) (Sinova et al., 2015). The magnitude of SHE spin current density is given by

$$j_S = j_e\theta_{SH}\hbar/2e, \quad \text{(Equation 4)}$$

where θ_{SH} denotes the spin hall angle, a coefficient that quantifies the strength of SHE. It is worth noting that the generated spin polarization vector points to the same direction regardless of whether it is derived from the Rashba-Edelstein effect and/or the SHE; even currently it is still ambiguous to rigorously differentiate and parse these two contributions to the charge-to-spin conversion (Fan et al., 2014a; Manchon et al., 2019; Yang et al., 2016). In fact, owing to the strong SOC with larger momentum $\boldsymbol{p}$, the heavy metal (HM) is extensively utilized in the experimental implementation systems of HM (Ta, Pt, W, etc.)/FM bilayers. To summarize, as illustrated in Figure 1D, the +/-$\boldsymbol{x}$-direction in-plane charge current ($\boldsymbol{j}_{e,x}$) in a strong SOC layer will generate a considerable interfacial spin current, i.e., a $\boldsymbol{z}$-direction spin current $\boldsymbol{j}_S^{\boldsymbol{y}}$ with the spin polarization vector along -/+$\boldsymbol{y}$, which brings SOTs onto its neighboring FM layer.

The generated SOTs acting on the precessional magnetization dynamics can be described by a similar form with Equation (1) as

$$\frac{d\boldsymbol{M}}{dt} = -\gamma \boldsymbol{M} \times \boldsymbol{H}_{eff} + \frac{\alpha}{M_s}\left(\boldsymbol{M} \times \frac{d\boldsymbol{M}}{dt}\right) + \frac{\gamma}{\mu_0 M_s}\boldsymbol{\tau}_{SOT}, \quad \text{(Equation 5)}$$

and both the $\boldsymbol{\tau}_{SOT}$ here and the $\boldsymbol{\tau}_{STT}$ in Equation (1) consist of a field-like term $\boldsymbol{\tau}_{FL} \sim \boldsymbol{m} \times \boldsymbol{\zeta}$ that makes $\boldsymbol{m}$ to precess around $\boldsymbol{\zeta}$ and a damping-like term $\boldsymbol{\tau}_{DL} \sim \boldsymbol{m} \times (\boldsymbol{\zeta} \times \boldsymbol{m})$ (Brataas et al., 2012; Manchon et al., 2019; Li et al., 2019; Zhang et al., 2017) that tends to align $\boldsymbol{m}$ along $\boldsymbol{\zeta}$, where $\boldsymbol{\zeta}$ is a unit vector determined by the incoming spin polarization. Particularly, $\boldsymbol{\zeta}$ points $\boldsymbol{z}$ direction in the PMA STT configuration as depicted in Figure 1A; however, $\boldsymbol{\zeta}$ aligns to $\boldsymbol{y}$ in the case of SOTs, as shown in Figure 1D. Hence, in contrast to the STT which damping-like term $\boldsymbol{\tau}_{DL}$ competes with the damping torque collinearly and thereby undergoes considerable precessions, the $\boldsymbol{\tau}_{DL}$ of SOT points perpendicular to the damping torque, as shown in Figure 1E, leading to much faster magnetization switching (Figure 1F) without the need of thermal fluctuation. The nonvolatile spin-orbitronic devices based on such SOC-originated transient magnetization dynamics are then capable of sub-nano second writing operations (which is comparable with the operation speed of a static random access memory, SRAM) with sub-picojoule energy consumption per bit (Garello et al., 2019b). Furthermore, the endurance and stability of the spin-orbitronic devices are much better than the spintronic devices based on STT-MTJ, owing to the separation of the relatively large in-plane writing current and the harmless small out-of-plane tunneling reading current in a three-terminal SOT-MTJ.

Upon a decade of fundamental research efforts, the spin-orbitronic devices based on SOT technologies are undergoing rapid development from laboratory investigations to engineering practice. In this perspective, first, the emerging applications of spin-orbitronic devices are specifically introduced. Then, we summarize the latest advancements in SOT research and highlight the main challenges for practical devices development. Finally, new opportunities for future spin-orbitronic devices in the new decade are discussed in detail.

EMERGING SPIN-ORBITRONIC DEVICES APPLICATIONS

The STT-based spintronic devices have already demonstrated their commercial value as recently announced mass production of the eMRAM to replace the existing NOR Flash embedded memories (Sato et al., 2018a). Owing to the consolidated superior performance, SOT-based spin-orbitronic devices

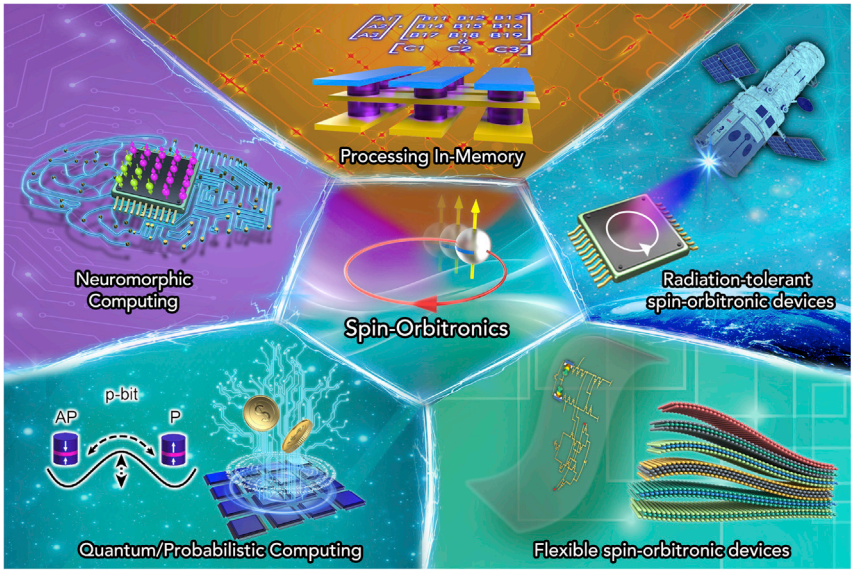

Figure 2. Schematics of Representative Emerging Spin-Orbitronic Device Applications

are naturally expected to complement and extend nonvolatile memory applications as SOT-MRAM. In addition, as human society steps into the era of big data, artificial intelligence, quantum computing, and internet of things, there are also promising opportunities for the nonvolatile spin-orbitronic devices with ultrafast dynamics controllability, excellent energy efficiency, almost unlimited endurance, outstanding stability, radiation resistance, and validated CMOS-compatibility to be explored in related emerging applications as exampled in Figure 2.

Processing in Memory

With the current von Neumann architecture, the conventional computation and storage are separately operated in the processor (i.e., a central processing unit, CPU) and the memory (i.e., static/dynamic random access memories, SRAM/DRAM), respectively. Data have to be transported frequently between the volatile CPU, SRAM, and DRAM and finally be stored in a nonvolatile hard disk drive, where there are deteriorating speed gaps between CPU and memory hierarchy units. In many cases, the data movement consumes even more time and energy than the computation. These "memory wall" or "von Neumann bottleneck" problems present to be a paramount hurdle to futuristic data processing computation, especially for the growing data-centric tasks, such as image and voice recognitions (Zidan et al., 2018). The concept of processing in-memory (or in-memory processing/computing) with stateful resistance-resistance (*R-R*) logics is then proposed to tackle the above issues by designing systems that implement computing within the memory (Ielmini and Wong, 2018). Typically, the nonvolatile memories with time- and energy-efficient processing capabilities are thereby extensively pursued. The candidates include memristor-based resistive switching RAM (RRAM) (Jo et al., 2010), phase change memory (PCM) (Kuzum et al., 2012), ferroelectric RAM (FeRAM) or tunnel junction (FTJ) (Mikolajick et al., 2001; Chanthbouala et al., 2012), and STT-as well as SOT-MRAMs (He et al., 2018). The RRAM and the PCM are usually regarded as potential candidates for in-memory processing owing to their large on/off ratio (resistance ratio between the high and the low resistance states, generally >1,000%) and feasibility of fabricating large crossbar arrays; however, their switching variability (including circle-to-circle or device-to-device variabilities) and resistance instability issues, together with their ambiguous underlaying physics, have to be addressed before being utilized for large-scale practical applications.

The SOT-MRAM demonstrates more competitive operation speed, resistance consistency, and energy efficiency performance, in particular the superior endurance characteristics. Remarkably, the endurance of an SOT-MTJ has been experimentally verified up to 10^{12} and can be as high as 10^{16} in theory (Baumgartner et al., 2017), making it specifically capable of processing applications, which requires much more rewriting operations than a generic data storage RAM. However, as one of the most promising building blocks for in-memory processing, spin-orbitronic SOT-MTJ devices are still facing major challenges to be completely

explored and utilized, such as the moderate on/off ratio and the three-terminal architecture nature. Briefly, the TMR value is defined as $(R_{ap} - R_p)/R_p$, where R_{ap} and R_p are the respective resistance when the magnetization of the free FM layer is antiparallel or parallel to the reference FM layer (Djayaprawira et al., 2005). Although 604% TMR was achieved in an in-plane MTJ (Ikeda et al., 2008), the typical TMR values for perpendicular CoFeB/MgO/CoFeB junctions are usually falling into a range of 100%–200%. Besides, the cell architecture and algorithm challenges in connecting the three-terminal SOT-MTJs have to be addressed with a similar form as conventional memristor crossbar arrays, which consist of multiple two-terminal memristive intersections between orthogonal row and column electrodes and thereby can realize parallel in-memory processing following the universal Kirchoff's law and Ohm's law. Considering this, novel designs of in-memory logic gates based on three-terminal SOT-MTJs (Wang et al., 2018d; Shreya et al., 2020; Zhang et al., 2020b), as well as attempts of two-terminal SOT-MRAM cells (Sato et al., 2018b; Wang et al., 2018a), have been demonstrated recently. As a concluding remark, the robust processing-in memory circuit with low standby power, re-configurable flexibility, and highly parallel computing characteristics are desired with unleashing spin-orbitronic memory and logic devices potential.

Neuromorphic Computing

Similar to in-memory processing, the neuromorphic computing is another non-von-Neumann processing approach, which aims specifically at solving artificial intelligence tasks with much better efficiency. Inspired by the working principle of human brain, a neuromorphic computing process involves the learning (or training) and the inference sections, and various working models including artificial/spiking/recurrent neuron networks (ANN/SNN/RNN) with respective algorithms have been proposed and established (Xia and Yang, 2019). The present developed learning processes are typically categorized into the supervised learning with large amount of labeled training samples, as well as the highly pursued unsupervised learning by clustering data without label (Wang et al., 2018c). Regardless of the above algorithm and circuits issues, from the device point of view, the primary artificial synapses and neurons are prerequisite components in building up a neuromorphic computing system generally.

In particular, an artificial synapse requires multilevel differentiated nonvolatile states, e.g., a memristive device, to store synaptic weights via implementing the analog of a variable resistor. Although spin-orbitronic devices show better performance indexes over other memristor candidates, however, the characteristic binary resistance nature of generic MTJ makes it difficult to proceed implementing as a multilevel synapse rather than a stochastic binary synapse (Grollier et al., 2020). One representative solution is to utilize the current-induced domain wall motion within the FM free layer (Sengupta et al., 2015a; Lequeux et al., 2016; Yue et al., 2019; Yang et al., 2019c; Siddiqui et al., 2019; Azam et al., 2020; Zhang et al., 2019b), for instance, by tuning the pinning potential of FM domain wall motions, SOT-induced multilevel magnetization switching as well as the typical synaptic functionality of spike-timing dependent plasticity (STDP) have been experimentally demonstrated (Cao et al., 2019). Other strategies include the fine-magnetic domain switching in antiferromagnetic (AFM) (Wadley et al., 2016; Olejník et al., 2017; Shi et al., 2020) or AFM/FM (Liu et al., 2020b; Zhou et al., 2020; Yun et al., 2020) heterostructures where multiple ~100 nm-sized binary FM domains fixed by the polycrystalline AFM could reverse independently under the applying current (Fukami et al., 2016; Kurenkov et al., 2017; Borders et al., 2016) and the SOT-induced skyrmion (a topological magnetic state) motions where the number of skyrmions within the signal reading area is proposed to represent the analog synaptic weight (Song et al., 2020a). In addition to the above efforts that try to form holistic multilevel magnetization by combining in-plane distributed binary magnetic solitons, which are difficult to achieve scalable multilevel spin-orbitronic synapses, the methodologies of innovating multilevel magnetization with out-of-plane multilevel mechanisms might be more practical and warrant more reliable solutions (Hong et al., 2018; Hu et al., 2020; Sheng et al., 2018b).

In parallel to synapses development, an artificial neuron receives and outputs stimulus signals from/to its multiple surrounding artificial synapses and adjusts their synaptic weights synchronously. As to the conventional ANN systems, the role of artificial neurons could even be replaced by setting nonlinear activation functions, whereas the SNN for unsupervised learning requires artificial neurons with leaky integrate-and-fire (LIF) (Stoliar et al., 2017; Chen et al., 2018d) behaviors that response occurs only at the integrated stimulus above a certain threshold. Electrically controlled spin-orbitronic devices with a clear critical magnetization switching current are therefore capable of mimicking such artificial neurons in principle (Diep et al., 2014; Sengupta et al., 2015b; Kurenkov et al., 2019), but the magnetization states of such nonvolatile neurons may have to be initialized after each fire. The volatile spin-torque nano-oscillator

(STNO) (Torrejon et al., 2017; Farkhani et al., 2019; Liang et al., 2020), a specific type of STT-MTJ that oscillates spontaneously with a low d.c. current-tunable precession amplitude and finite magnetization relaxation, has recently been experimentally demonstrated as an efficient artificial neuron for speech recognition owing to its stability, low noise, and high nonlinearity of frequency and amplitude. As the spin-orbitronic version of STNO, spin hall nano-oscillators (SHNOs) had been also developed to implement as neurons (Sato et al., 2019; Zahedinejad et al., 2020); however, as depicted in Figure 1E, the relationship between the magnetic damping and the SOT-induced in-plane damping-like torque in a PMA-FM is not as symmetrical as the case of STT shown in Figure 1B; hence, challenges and new opportunities coexist in proposing such an artificial neuron based on the PMA SHNO (Fulara et al., 2019) in the absence of an in-plane magnetic field. Moreover, the demonstration of new bio-inspired neurons should also provide new opportunities beyond current neuromorphic computing principles, for example, to realize the logic gate of exclusive OR (XOR) in a single spin-orbitronic device, which can imitate the newly found linearly nonseparable input-output behaviors of layer 2/3 pyramidal neurons in human brain and thereby offers novel intelligent functionalities (Gidon et al., 2020). Besides, further algorithms and interconnection innovations are also desired for future practical large-scale neuron networks based on spin-orbitronic synapses and neurons.

Probabilistic Computing

Connecting the classical digital computing based on deterministic bits of 0 or 1 and the quantum computing based on quantum bits (q-bits) with coherent superpositions of 0 and 1, there is an intermediate approach of probabilistic computing that relies on sampling probabilistic bits (p-bits) with spontaneously fluctuated states of either 0 or 1 (Chowdhury et al., 2019). In the current new era of noisy intermediate-scale quantum (NISQ) technology, a period that the noise in quantum gates limits the size of quantum circuits (Preskill, 2018), which is far from the eventually accurate, fully fault-tolerant quantum technologies in the future, the probabilistic computing with interconnected p-bits can be practically useful in a host of quantum computing applications, such as solving satisfaction, optimization (e.g., the traveling salesman problem, the integer factorization, and the invertible logics), and sampling problems (Sutton et al., 2017; Grollier et al., 2020). The hardware construction of p-bit can be exactly realized by utilizing the low-barrier nanomagnet (LBNM), a single domain magnet or superparamagnetic particle whose magnetization reverses randomly when the barrier between opposite magnetic states is comparable with the thermal energy ($H_K M_s V/2 \approx k_B T$, where the five quantities are the anisotropy field, the saturation magnetization, the volume, the Boltzmann constant, and the absolute temperature, respectively) (Camsari et al., 2017). MTJ with an LBNM as its free layer has been demonstrated as a high-speed p-bit, the time average state (resistance) of which can be modulated by an electric current via STT or SOTs (Borders et al., 2019; Debashis et al., 2020), and the hardware Boltzmann machines with stochastic neuron networks consisting of such asynchronously tunable correlated p-bits are thereby capable of searching the vast phase space of hard problems by utilizing the modified adiabatic quantum computing algorithms. Unlike the existing delicate q-bits that generally work at ultralow temperature for quantum computing, such LBNM-based p-bits work at room temperature and can be convincingly modified from the market-ready MTJ technology. Nevertheless, the performance reproducibility of LBNMs should be enhanced and further investigations on zero-field SOT-induced modulation of a PMA LBNM are also expected with the involvement of multidisciplinary fields.

In a broad sense, spintronic probabilistic devices are not limited to the fluctuated LBNMs. The stochastic behaviors can also be found in non-deterministic current-induced magnetization switching processes (Grimaldi et al., 2020), enabling to be exploited for probabilistic computing. Particularly, since thermal activation plays an important role in the STT-induced switching dynamics, the magnetization is not amenable to be switched at a low current regime and the switching probability increases with growing current density and pulse duration. Interestingly, the STT-based stochastic synapses and neurons performing with short and low current pulses are then proposed to reduce the energy consumption of a neuron network (Sengupta et al., 2016; Ignatov et al., 2017; Vincent et al., 2015). The SOT-induced switching of a PMA-FM possesses unique stochasticity, where the switching probability of a specific switching sense (i.e., a down → up or an up → down magnetization switching for a fixed j_x) depends on the direction and the magnitude of external in-plane magnetic field applying along the current channel. In the absence of external magnetic field, in principle, there should be a perfectly 50%:50% chance for a PMA-FM (regardless of the initial magnetization state) to switch toward either the down or the up magnetization state, which makes single domain PMA SOT device a natural binary true random number generator (TRNG) (Kim et al., 2015; Liu et al., 2018; Chen et al., 2018a). Besides, the physical unclonable functions (PUFs) (Gao et al., 2020) can also be

proposed by a matrix of PMA spin-orbitronic devices with the above non-deterministic zero-field SOT switching properties (Finocchio et al., 2019), which provides additional advantages over other PUF technologies in non-volatility, reconfigurability, and scalability toward the new type of keystone for maturing probabilistic computing. Further out on the roadmap with certain achieved milestones, the promise of probabilistic computing is intriguing, while it is apparently still at its infancy stage. The ultimate goal is to aim to realize probabilistic computing with reliable spin-orbitronic devices-based hardware realization from algorithms to predictive circuit models.

Avionics and Internet of Things

In the short term, rather than challenging the stand-alone memories such as Flash and DRAM, which possess the steady productions and complete supporting software, the emerging spin-orbitronic devices are gaining momentum and finding their priorities in the embedded nonvolatile memory market, such as emerging applications in the fields of avionics and internet of things (IoT), which are requiring processing and memory at the edge of advanced networks as well as at the endpoints. Particularly, the devices used in the aerospace are required to be radiation resistant to cosmic rays. Since MTJs are equipped with intrinsic magnetic immunity to radiation effect (Kobayashi et al., 2014; Hughes et al., 2012; Ren et al., 2012; Park et al., 2019), MRAMs have already been used in satellites early in March 2008 (Greenemeier, 2008). Moreover, featured with almost unlimited endurance, spin-orbitronic devices are particular favorable to be applied in avionics, e.g., a spacecraft, which may travel more than tens of years in the universe.

On the other hand, IoT is a compelling platform connecting trillions of smart objects for sensing, collecting, memory, analyzing, and communication. The stability, endurance, and energy efficiency are generally concerned for the edge equipment connected in an IoT system, and all these requirements could be exactly fulfilled with applicable spin-orbitronic devices (Liu et al., 2019d). In addition to the magnetoresistance sensors that have already been widely used, sub-field researches on novel spin-orbitronic devices are desired for versatile specific IoT applications, including flexible SOT devices for wearable equipment (Lee et al., 2015), SOT-driven antiferromagnetic memories for security and magnetic field-immune applications, as well as spin-orbit THz emitters utilizing the ultrafast spin dynamics and the inverse spin Hall effect (ISHE) in FM/HM bilayers for rapid data communications (Kampfrath et al., 2013; Seifert et al., 2016; Wu et al., 2017). Besides, spin-orbitronic devices based on MTJs could also harvest the heat dissipation on a chip or from the environment and generate sufficient thermopower by magneto-Seebeck effects (Liebing et al., 2011; Walter et al., 2011; Boehnke et al., 2017; Tu et al., 2020; Friesen et al., 2019). In summary, the discovery of SOT-induced electrical manipulation of ferromagnet may be just a beginning and the party of spin-orbit related researches and applications will continue to prosper.

KEY CHALLENGES FOR SPIN-ORBITRONIC DEVICES

Realizing Field-free SOT Switching in a Scalable Way

As illustrated in Figure 1E, the +/-y-polarized spin current-induced $\boldsymbol{\tau}_{DL}$ alone will eventually align the magnetic moment $\boldsymbol{m}_z$ toward in-plane (+/-y-direction) orthogonal to the electric current (-/+x-direction); hence, an external in-plane magnetic field $\boldsymbol{H}_x$ is generally essential and prerequisite to break the symmetry and thereby realize the deterministic SOT-induced magnetization switching of PMA free layer in HM/FM structures (Emori et al., 2013). However, it is not applicable to introduce "bulky" and dissipative magnets into an SOT-MRAM for generating an assistive in-plane magnetic field, which goes counter to the demanding trend of data scalability and energy efficiency. As summarized in Figure 3, some representative symmetry breaking methods via generation or engineering of either magnetic field $\boldsymbol{H}_x$, magnetic anisotropy $H_K M_s/2$, or spin-orbit current $\boldsymbol{j}_S$, had been proposed to demonstrate magnetic field-free SOT-induced perpendicular magnetization switching. They are categorized as following four major schemes.

By Embedding the H_x within the Stacks

"T-type" magnetically coupled stacks consisting of a PMA-FM free layer and an in-plane FM or AFM pinning layer were designed, wherein the in-plane interlayer exchange coupling field (i.e., HM/PMA-FM free layer/spacer layer/in-plane FM pinning layer structure) (Lau et al., 2016; Sheng et al., 2018a; Bekele et al., 2020; Cao et al., 2019) or the in-plane exchange bias field (e.g., HM/FM/AFM structure or AFM/FM bilayer when the AFM is a strong SOC alloy such as PtMn or IrMn and thereby also works as the spin-orbit current source) (Fukami et al., 2016; Oh et al., 2016) acting on the PMA-FM free layer plays as a built-in assistive magnetic field for a deterministic SOT-induced magnetization switching.

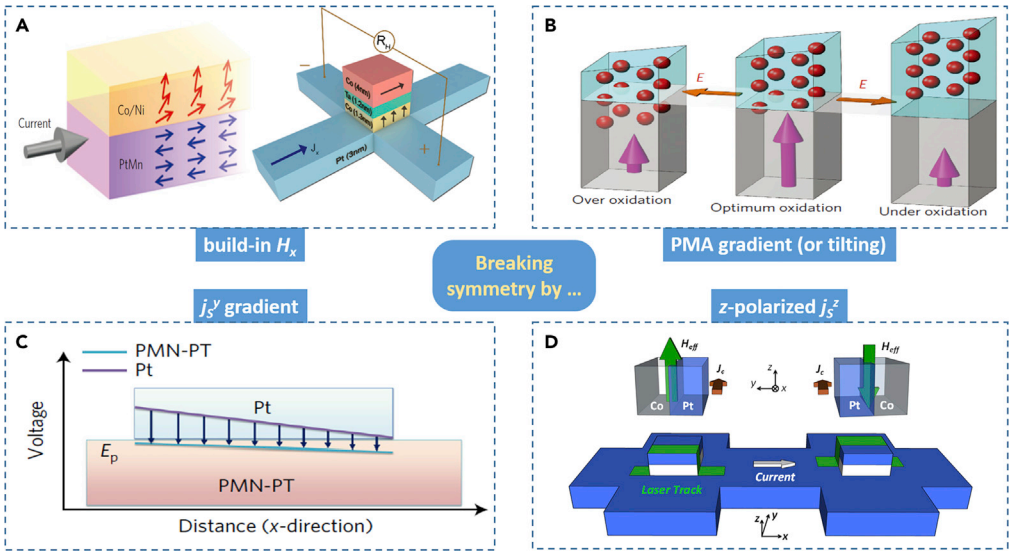

Figure 3. Strategies for Realizing Magnetic Field-free SOT Switching

Representative symmetry breaking methods via generation or engineering of either (A) magnetic field H_x (Fukami et al., 2016; Cao et al., 2019), (B) magnetic anisotropy (Yu et al., 2014), or (C and D) spin-orbit current j_S (Cai et al., 2017; Cao et al., 2020).

By Engineering the Spatial Asymmetry in the Magnetism (e.g., H_K or m_z)

Magnetic field-free SOT switching was reported in samples containing either a wedged HM layer, a wedged FM layer, or a wedged oxide capping layer with spatial gradient thicknesses (Chen et al., 2018c; You et al., 2015; Wu et al., 2020a; Yu et al., 2014). Although the exact mechanism remains unclear (Akyol et al., 2015), a gradient of the PMA or the saturation magnetization was thought to be responsible for the deterministic SOT switching. In other cases, the easy axis of the PMA-FM was tilted away from the out-of-plane direction either by annealing the sample under an in-plane magnetic field (Kong et al., 2019) or by epitaxially depositing the $SrIrO_3/SrRuO_3$ bilayer with tilted magnetocrystalline anisotropy on a (001)-oriented $SrTiO_3$ substrate (Liu et al., 2019c). Among them, each engineering methodology warrants sufficient asymmetry in the PMA for the field-free SOT-induced magnetization switching.

By Creating a Spin Current Gradient dj_S^y/dx

Hybrid ferroelectric (FE, such as PMN-PT) substrate/HM/PMA-FM stack structures were used to generate a gradient j_S^y when the FE was electrically polarized parallel with the electric current (***x***-direction) (Cai et al., 2017; Yang et al., 2019b). The conventional HM/PMA-FM devices constructed with a wedged HM thickness or an in-plane wedge-patterned channel can also lead to a gradient j_S^y via the gradient electric current (Chen et al., 2019a; Yang et al., 2019a). Such ***x***-direction gradient in j_S^y produces an additional torque $\sim \boldsymbol{M}\times(dj_S^y/d\boldsymbol{x})$ to the LLG equation and results in deterministic magnetization switching.

By Using an Out-of-Plane Polarized Spin-Orbit Current j_S^z Instead of the Conventional In-Plane Polarized j_S^y

Deterministic current-induced magnetization switching was obtained in an in-plane FM/Ti/PMA-FM structure where a ***z***-polarized spin-orbit current j_S^z was generated from the in-plane FM/Ti interface via spin-orbit precession (Baek et al., 2018a). It was also reported that the spin-orbit current from low symmetry Weyl semimetals (e.g., WTe_2 and $MoTe_2$) show out-of-plane spin polarization vectors (Macneill et al., 2017; Song et al., 2020b), whose effectiveness to a field-free magnetization switching for PMA-FMs remains to be experimentally examined. Zero-field current-induced magnetization switching was also demonstrated by combining the STT and the SOT, the interplay of which gives a compromised solution that shows better switching speed than the pure STT scheme, as well as allows the design of a two-terminal SOT-MTJ (Sato et al., 2018b; Wang et al., 2018a). However, the switching contribution from the perpendicular STT current and its damage to the fragile tunneling barrier have to be balanced. Most recently, a novel lateral SOT was

demonstrated in locally laser annealed Pt/Co/Pt trilayers, where j_S^z was generated from the laser-induced lateral local Pt-rich region inside the nominal Co layer (Cao et al., 2020). The current-induced an out-of-plane effective field and thereby zero-field magnetization switching was then achieved, the switching sense of which depends only on the relative location of the Pt-rich and the Co-rich regions, regardless of the net spin polarization of external spin current from both the bottom and the top Pt layers. The complementary spin-orbit building blocks analog to the n- and p-type semiconductors were then demonstrated by using a pair of lateral SOT devices with opposite laser annealing locations (Zhang et al., 2020a).

Despite the successful laboratory demonstration of the above proposals for field-free SOT-induced magnetization switching, however, the further high-demanding optimization on the their industrial applicability is required since most of these methods involve either an in-plane FM, a canted magnetization in the PMA-FM, unconventional device shapes or structures, or multiterminal (terminal number >3) devices, which may challenge the fabrication feasibility or data scalability of an external field-free SOT-MRAM. Competing spin currents from the Pt/W bilayers with opposite signs in the spin Hall angle was reported as an integration-friendly method for realizing field-free SOT induced magnetization switching in Pt/W/PMA-FM structures with proper Ta and Pt thicknesses (Ma et al., 2018), but the underlying mechanism is still unclear (Chen et al., 2020a; Wu et al., 2020b), which is hard to gain deeper insights into any of the above four symmetry breaking ways. Most recent data on deterministic SOT-induced magnetization switching by inserting a slightly asymmetric light-metal layer between the HM and the FM interface was also claimed as a quite scalable approach, the exact explanation of which remains elusive as well (Razavi et al., 2020), since counter-intuitive uniform PMA was observed across all devices on the wafer. New CMOS process compatible approaches and strategy along with plausible understandings of field-free spin-orbitronic devices physics are urgently desired to be explored.

Enhancing the Energy Efficiency by Materials Engineering

For a spin-orbit memory cell with given device size, the energy consumption per writing operation scales with $j_e^2 \rho t$, i.e., the square of critical switching current density, the resistivity of SOC layer, and the effective duration of switching pulse. The last term "t" can be reduced by replacing the FM with AFM systems such as synthetic AFMs and compensated ferrimagnets (Zhang et al., 2018; Cai et al., 2020), which shows much faster switching and domain wall motion speed. Anyway, in conventional HM/FM (HM = Pt, Pd, Ta, W, Hf, etc.; FM = Co, CoFe, CoFeB, etc.) structures, the j_e, which are generally reported as 10^6–10^8 A/cm^2 are highly requiring to be reduced to achieve better energy efficiency. In particular, the PMA strength and the damping-like SOT efficiency are two contrary factors that determine the j_e, and the damping-like SOT efficiency in an HM/FM system scales with the charge-to-spin conversion efficiency (represented by the spin Hall angle θ_{SH}, as aforementioned in the Introduction section) in the HM as well as the interfacial spin transparency (T_{int}) between the HM and the FM, at the interface of which the spins may be reflected (Zhang et al., 2015) or depolarized (Rojas-Sánchez et al., 2014; Tao et al., 2018; Zhu et al., 2019a). Therefore, enhancing the effective spin Hall angle $\theta_{SH,eff} = \theta_{SH} T_{int}$ via materials and device engineering is considered as a key solution to improve the energy efficiency of spin-orbitronic devices, as summarized below.

By Modifying the HM Layer and the Interface

It is worth noting that the $\theta_{SH,eff}$ must be balanced with the resistivity ρ, hence an approximate figure of merit (FOM) for the switching power density $P_{SW,FOM} \sim \rho/(\theta_{SH,eff})^2$ was suggested for estimating the overall power consumption per cross area (Manchon et al., 2019). Therefore, among conventional HMs that are commonly used for SOTs, Pt with moderate θ_{SH} but much smaller resistivity is more favorable than Ta and W. But the measured θ_{SH} (or $\theta_{SH,eff}$) values from Pt in the range of 0.37%–14% should be further increased for practical application (Kimura et al., 2007; Ganguly et al., 2014; Nguyen et al., 2016a; Rojas-Sánchez et al., 2014; Nakayama et al., 2013; Liu et al., 2011; Althammer et al., 2013; Choi et al., 2017). Considering that the intrinsic θ_{SH} in a *5d* metal increases proportionally with the resistivity due to enhanced scattering, impurities such as Al, Hf, Au, and MgO were doped as scattering centers into the Pt layer, where enhanced Pt resistivity and consequently the strengthened SOTs were obtained (Nguyen et al., 2016b; Zhu et al., 2018, 2019c). Other resistivity engineering methods, including adjusting the HM thickness (Nguyen et al., 2016a) or adjusting the deposition conditions (Zhang et al., 2016a; Lee et al., 2017) were also examined to be effective in promoting the SOT efficiency. It is noteworthy that the interface-originated spin-orbit current is supposed to be an important contribution factor to significantly enhance SOTs with Pt resistivity slightly increased, since more current is concentrated near the Pt/FM interfaces. The interfaces were further confirmed as prominent sources for generating substantial SOTs in Pt(O)/FM, W(O)/FM,

NiFe/Cu(O), Pt/CoFeB/MgO/SiO_2, and Pt/Co/TiO_x structures with highly resistive or insulating oxygen-incorporated metals (An et al., 2016, 2018b; Qiu et al., 2015; Bekele et al., 2018; Demasius et al., 2016). More specific interface modifications by using Cu, Ti, or Hf insertion layers between the HM and the FM layers were also performed (Rojas-Sánchez et al., 2014; Huang et al., 2015; Lee et al., 2019; Shi et al., 2018; Zhu et al., 2019b), where improved interfacial spin transparency T_{int} and thereby enhanced $\theta_{SH,eff}$ were obtained. Besides, the oxide/HM interface can also contribute to the overall SOTs in an oxide/HM/FM structure in terms of efficiency and direction (Sheng et al., 2019; Li et al., 2020).

By Using Strong SOC Materials Other than HM

In addition to HMs, HM-based alloys, and metal oxides, various alternative materials including semiconductors, van der Waals crystals, and topological materials have been proposed as potential spin-orbit-induced spin current sources; the highly relevant literature reported on $\theta_{SH,eff}$, ρ, and $P_{SW,FOM}$ are summarized in Table 1. Particularly, in semiconductor/FM heterostructures such as GaAs/Fe and paramagnetic (Ga,Mn)As/Fe bilayers, SOTs that originated at the interfaces were elucidated in detail (Chen et al., 2016, 2018b). Some layered van der Waals crystals also exhibit strong SOC and an appreciable range of broken crystal symmetries; most recently, the strong spin-orbit current and efficient SOTs were observed in transition metal chalcogenide (TMD)/FM heterostructures involving MoS_2 (Xie et al., 2019), WSe_2 (Shao et al., 2016), Dirac semimetal $PtTe_2$ (Xu et al., 2020), or Weyl semimetal WTe_2 (MacNeill et al., 2017; Shi et al., 2019; Li et al., 2018; Zhao et al., 2020) and $MoTe_2$ (Song et al., 2020b). Topological insulators (TIs) of $Bi_{1-x}Sb_x$ and their chalcogenides (X_2Q_3, X = Bi, Sb, $Bi_{1-x}Sb_x$; Q = Se, Te) with strong spin-momentum locking in the conductive surface are expected as promising source of SOTs (Khang et al., 2018; Wang et al., 2017; Mahendra et al., 2018; Chen et al., 2020b; Han et al., 2017). The reported θ_{SH} in such TIs can exceed 100%, offering the superior efficiency of the SOTs over the STT, which bears the limited charge-to-spin conversion efficiency 100% in maximum. Highly efficient SOT-induced switching of perpendicular magnetized MnGa with a $j_e = 1.5 \times 10^6$ A cm^{-2} was observed by using conductive topological insulator $Bi_{0.9}Sb_{0.1}$ thin film with a high conductivity (>2.5×10^5 $\Omega^{-1}m^{-1}$) and a large $\theta_{SH,eff}$ (~5,200%) (Khang et al., 2018). In the case of a sputtered Bi_xSe_{1-x}/CoFeB bilayer on the Si/SiO_2 wafer (Mahendra et al., 2018), the j_e had been lowered to as low as 4.3×10^5 A/cm^2. The open questions for these TI-based spin-orbitronic devices keep remaining, including the challenge in reproducible large area industrial fabrication, the structurally and chemically thermal stability, the compatibility with PMA-FM, and the issues at the interface where the uncertainty in TI surface conductivity as well as the possible interfacial orbital hybridization or chemical changes have to be considered.

Integration Challenges

Nowadays, the spin-orbitronic devices are encountering major on-chip integration challenges pertaining to scaling compatibility, energy efficiency, interfacing circuit design, etc., which challenge both two-terminal and three-terminal schemes in device, cell, and system levels. Among them, one typical challenge is the integration of SOT-MTJ with CMOS, where there is an extra SOC layer compared with an STT-MTJ. Briefly, a CMOS-compatible SOT-MTJ process flow is as follows. Upon availability of high-quality MTJ stacks consisting SOC layer via employing physical vapor deposition (PVD, e.g., sputtering), specifically designed SOT-MTJ masks are required to define the MTJ element pillar using deep immersion (e.g., 193 nm) lithography before the etching module by ion beam etching. Note that the quality and fabrication reproducibility of the stacks primarily depend on the properties of the SOC layer, FM free layer, and barrier layer, as well as interfaces formed in the module. The dedicated chamber with atomic level precision (~0.1 Å) one-step deposition helps to improve films quality control, i.e., stoichiometry, integrity, defectivity, and uniformity, eventually to reproducibly achieve the target SOT and magnetization switching efficiency, resistance-area product, and TMR characteristics (Qiu et al., 2018; Ramaswamy et al., 2018). Typically, the top pinned MTJ consists of SOC layer/CoFeB/MgO/CoFeB/SAF perpendicularly magnetized stacks, where typical β-W or Ta-based electrode works as SOC layer (Garello et al., 2019a). Hence, specific stop etching conditions have to be developed to enable the SOC layer intact with dedicated endpoint detection mode while patterning the MTJ pillar without producing re-deposition clusters, which would form sidewall shorts across the MgO barrier layer. Subsequently, the SOC layer is etched to form the two or three terminals device, and the gap filling is to be implemented following with chemical mechanical planarization. Also note that most recently reported SOTs in various single magnetic layers could help to facilitate the development of SOT-MTJs without the SOC layer (Wang et al., 2012; Amin et al., 2019; Luo et al., 2019b; Liu et al., 2020a; Zhang et al., 2020a; Tang et al., 2020; Cao et al., 2020). Eventually, a dual damascene Cu or TiN electrode will be fabricated to complete the electrical connection for routing and testing.

Materials	θ_{SH} (%)	ρ (10^{-8} Ω m)	$P_{SW,FOM}$ (10^{-5} Ω m)	Method	Reference
Metals					
Pt	0.37	15.6	1,139.52	NLD	(Kimura et al., 2007)
	2.2	28	57.85	ST-FMR	(Ganguly et al., 2014)
	4	86	53.75	SMR	(Nakayama et al., 2013)
	5.6	20	6.38	ST-FMR	(Liu et al., 2011)
	5.6	17.3	5.52	SP	(Rojas-Sánchez et al., 2014)
	8.5	28	3.88	DC	(Ganguly et al., 2014)
	11	32.8	2.71	SMR	(Althammer et al., 2013)
	12	50	3.47	SHM	(Nguyen et al., 2016a)
	14	31	1.58	SMR	(Choi et al., 2017)
Pd	0.8	27	421.88	ST-FMR	(Kondou et al., 2012)
	1.2	20	138.89	SP	(Vlaminck et al., 2013)
α-Hf	7[a]	156.25	31.89	SMR	(Liu et al., 2015)
Hf	11[a]	400	33.06	SMR	(Liu et al., 2015)
β-Ta	−12	190	13.19	ST-FMR	(Liu et al., 2012)
	−7.1	290	57.53	SP	(Wang et al., 2014)
β-W	−14	180	9.18	SP	(Wang et al., 2014)
	−22	129	2.67	SMR	(Choi et al., 2017)
	−30	300	3.33	ST-FMR	(De La Venta et al., 2013)
	−40	210	1.31	SP	(Hao and Xiao, 2015)
Metal alloys					
$Pt_{80}Al_{20}$	14	75	3.83	SHM	(Nguyen et al., 2016b)
$Pt_{85}Hf_{15}$	16	110	4.30	SHM	(Nguyen et al., 2016b)
$Pt_{75}Au_{25}$	35	80	0.65	SHM	(Zhu et al., 2018)
Metal oxides					
$W_{88}O_{12}$	−49	172	0.72	ST-FMR	(Demasius et al., 2016)
PtO_2	92	~ 10^9	~ 10^6	ST-FMR	(An et al., 2018a)
Antiferromagnets					
PtMn	6	164	45.56	SP	(Zhang et al., 2014)
FeMn	0.8	167.7	2,620.31	SP	(Zhang et al., 2014)
PdMn	1.5	223	991.11	SP	(Zhang et al., 2014)
IrMn	2.2	269.3	556.40	SP	(Zhang et al., 2014)
	22	205	4.24	ST-FMR	(Tshitoyan et al., 2015)
$IrMn_3$ (001)	20	160	4.00	ST-FMR	(Zhang et al., 2016b)
$IrMn_3$ (111)	12	198	13.75	ST-FMR	(Zhang et al., 2016b)

Table 1. The Signed Spin Hall Angle θ_{SH}, the Resistivity ρ, and Calculated Figure of Merit of the SOT Switching Power Density $P_{SW,FOM} \sim \rho/(\theta_{SH,eff})^2$ for Various Materials at Room Temperature

(Continued on next page)

Materials	θ_{SH} (%)	ρ (10^{-8} Ω m)	$P_{SW,FOM}$ (10^{-5} Ω m)	Method	Reference
Semiconductors					
(Ga,Mn)As	0.15	4,300	1.91×10^{6}	SP	(Mendes et al., 2017)
2D semimetals					
WTe_2	51	580	2.23	ST-FMR	(Shi et al., 2019)
$MoTe_2$	3.2	550	537.11	ST-FMR	(Stiehl et al., 2019)
$PtTe_2$	15.2	95	4.11	ST-FMR	(Xu et al., 2020)
TIs					
Bi_2Se_3	16	1,060	41.41	DC	(Han et al., 2017)
	175	4,117	1.34	ST-FMR	(Wang et al., 2017)
Bi_xSe_{1-x}	1,870	12,821	0.04	DC	(Mahendra et al., 2018)
	867	12,821	0.17	ST-FMR	(Mahendra et al., 2018)
$(Bi,Sb)_2Te_3$	40	4,020	25.13	DC	(Han et al., 2017)
$Bi_{0.9}Sb_{0.1}$	5,200	400	1.48×10^{-4}	DC	(Khang et al., 2018)

Table 1. *Continued*

TIs, topological insulators; Method, measuring method; NLD, non-local detection; ST-FMR, spin torque ferromagnetic resonance; SMR, spin Hall magnetoresistance; SP, spin pumping; DC, direct current method; SHM, second-harmonic measurement.

[a]Sign uncertain.

Benefiting from the matureness of STT-MTJ development (He et al., 2018), the established process know-how gained from STT-MRAM foundries learning cycles are constructive to tackle the existing integration obstacles of SOT-MRAM. Examples include the elemental movements and morphology changes impact on perpendicular magnetic anisotropy and exchange coupling degradation, as well as the strong dependence of the magnetoresistance and reliability on the defect species and concentration, diffusion barrier and interface quality of SOT and MTJ modules, etc. However, owing to the unique device structure for strong SOC-induced SOT-driven magnetization switching implemented with synergistic MTJ integration during back-end of line (BEOL) process, SOT-MTJ bears special process integration and control challenges (e.g., the dimension, thickness, and smoothness of heavy metal and corresponding thermal stability with the co-optimized spin hall angle and conductivity), which engages specific engineering needs for electrodes, film stack, lithography, alignment accuracy, etching process, clean technology, and encapsulation with applicable low-k gap filling, etc. For instance, compared with STT-MRAM thin films, to develop a robust wafer-level thin film process for SOT-MRAM with high thermal stability remains a great challenge upon maintaining MTJ perpendicular anisotropy after 400°C thermal budget during typical CMOS integration. Hence, it is indispensable to build up a robust SOT-MRAM fabrication integration process to enhance the thermal stability of the SOT-MRAM (Ramaswamy et al., 2018; Garello et al., 2019a). Furthermore, in order to successfully move SOT-MRAM into pre-industrial maturity phase, it is also expected to tackle aforementioned emerging integration issues with BEOL thermal budget compatibility and critical switching current minimization, which would in turn mitigate the current existing indecisive concern on the device modeling, circuit simulation, and system level integration development momentum for spin-orbitronics devices including SOT-MRAM.

THE FUTURE OPPORTUNITIES

Parallel to the intensive investigations on the above challenges, the research community of spin-orbitronic devices are moving on for future science and technologies. Corresponding to an estimated timescale from near technology improvement to farther future principle innovations, here we example the 3D SOT-MRAM, the programmable spin-orbit logics, and the exotic magnetic configurations with new physics to be rising highlights in the field of spin-orbitronics, as following.

3D SOT-MRAM

Energy-efficient nonvolatile memory plays a paramount important role in the implementation of artificial intelligence and advanced network technologies at the endpoints. An increasing demand for massive

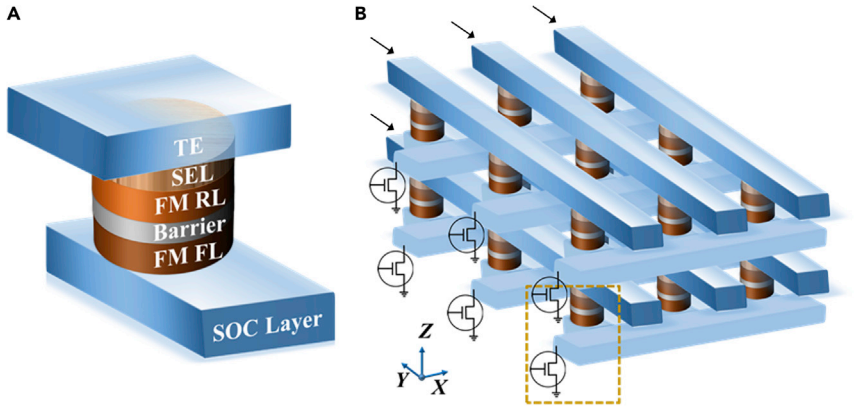

Figure 4. A Proposed 3D SOT-MRAM

Schematic of proposed single two-terminal SOT-MTJ cell (A) and the corresponding integrated 3D SOT-MRAM architecture (B). Writing and reading currents can be addressed to a specific MTJ cell by controlling the transistor switches and selectors. FL, free layer; RL, reference layer; SEL, selector; TE, top electrode.

and variable data storage and fast processing (e.g., autonomous vehicle applications) drives 3D memory integration to be a key enabler, and thus bringing the scaling concept to the next level of the system requirements (Chandrasekaran, 2013). The major semiconductor design house and industrial foundry players are engaged in developing 3D-MRAM product equips a class of nonvolatile memory arrays that are scalable to be stacked to achieve complementary DRAM performance and Flash non-volatility attributes with high density (Huai et al., 2018).

Poised as a keystone architecture, 3D cross-point SOT-MRAM is one of the best candidates as two-pronged approach of 3D STT-MRAM to replace eDRAM, for instance, and serve as the storage class memory (SCM). Aiming at achieving both high-density and high-performance 3D SOT-MRAM, herein a two-terminal stackable 3D cross-point field free SOT-MRAM architecture is proposed, comprising an integrated selector in series with perpendicular MTJ. As illustrated in Figure 4, an optimized prerequisite 1-transistor-1-resistor (1T1R) device configuration is made of interrelated SOC layer with large spin Hall angle and high spin conductivity, enabling significant enhancement of SOT-driven magnetization switching efficiency in FM free layer of MTJ. Importantly, both in-plane and out-of-plane currents are simultaneously generated on application under a programmable bias voltage; nevertheless, the SOT switching mechanism is prerequisite to facilitate compact and highly efficient operation (Sato et al., 2018b). Moreover, in the two-terminal stacked 3D SOT-MRAM array, to eliminate the sneak current induced cross-talk issue through the half-biased unselected cell in the same row or column of the selected element, an applicable selector is required with low ON voltage $V_{ON} < 1$ V, fast turn-on and turn-off speed (<1 ns), as well as the suppression capability of non-linearity ratio (i.e., the ratio between the maximum current J_{ON} and the current $J_{HB} = J(^1/_2V_{ON})$ of half biased cells) in a memory-type SCM, for instance. In fact, as demonstrated from the latest reports, the timely overall performance investigation of stacked SOT-MRAM architecture in comparison with other memory technologies in array and hybrid level elaborates its superior area, access latency, access energy, and write current benefits (Moradi et al., 2019; Bishnoi et al., 2014). Hence, it enables the access transistor(s) of an SOT-MRAM bit-cell to be designed much smaller, in turn leading to a lower leakage power for 3D SOT-MRAM.

Programmable Spin-Orbit Logics

In contrast to the field free SOT-induced deterministic magnetization switching of $\boldsymbol{m}_z$, the unwanted external $\boldsymbol{H}_x$ that requires for breaking symmetry can turn out to be a unique advantage of reconfiguring the switching sense, since the direction of $\boldsymbol{H}_x$ determines a down → up or an up → down orientation of the $\boldsymbol{m}_z$ for a fixed $\boldsymbol{j}_x$. Corresponding to the aforementioned strategies for realization of external $\boldsymbol{H}_x$-free SOT-induced $\boldsymbol{m}_z$ switching, the programmable spin-orbit cells for memory and logic applications with increased logic densities are desired in various reversable symmetry breaking ways. One basic idea is to adjust the interlayer coupling field direction by magnetically or electrically pre-magnetizing the in-plane FM pinning layer within the "T-type" magnetically coupled HM/PMA-FM free layer/spacer layer/in-plane

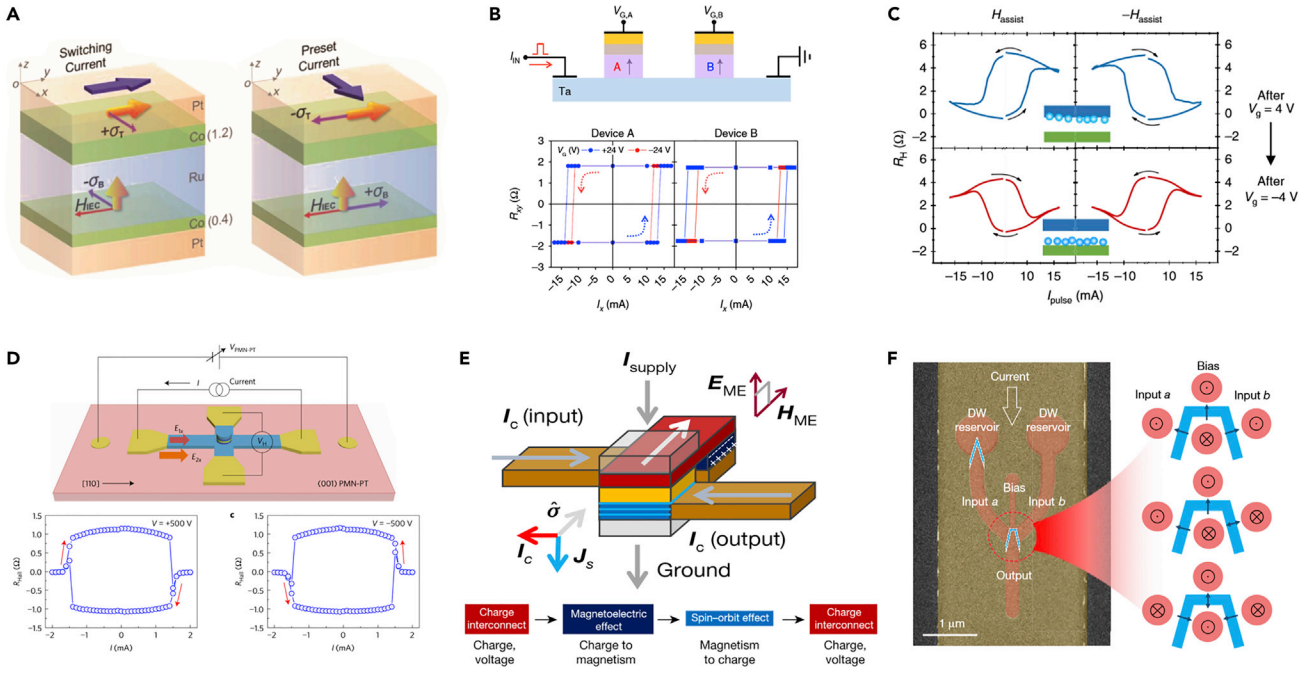

Figure 5. Devices for Programmable Spin-orbit Logics

Representative reprinted works reported on, or potentially capable of, demonstrating programmable spin-orbit logics based on various device approaches, e.g., (A) reconfigurable SOT switching of the PMA-FM layer in a "T-type" magnetically coupled structure realized by tuning the magnetization direction of the assistant in-plane FM layer via in-plane configured SOTs by applying orthogonal electrical currents (Wang et al., 2018b).

(B) VCMA control of the PMA and thereby the driving current intensity of the SOT switching (Baek et al., 2018b).

(C) Tuning the polarity of current-induced spin accumulation by modulating the oxygen ions in a Pt/Co/GdO_x structure by voltage gating, the interfacial chemistry of which results in an interplay between the interfacial torques and the spin Hall current from Pt, and determines the sense of the SOT-induced magnetization switching (Mishra et al., 2019).

(D) External magnetic field-free reconfigurable SOT switching of Pt/CoNiCo/Pt obtained by electrically controlling the nonvolatile polarity of the ferroelectric PMN-PT substrate, where sufficient gradient in spin-orbit current is produced, and the direction of which determines the SOT switching sense to be clockwise or anticlockwise (Cai et al., 2017).

(E) MESO devices involving the magnetoelectric effect and the charge-to-spin interconversions via spin filter and spin-obit effects (Manipatruni et al., 2019).

(F) Reconfigurable and cascadable SOT-induced magnetic domain-wall logics by exploiting the invertible chiral coupling between neighboring magnetic domains (Luo et al., 2020).

FM pinning layer stacks (Sheng et al., 2018a; Wan et al., 2017; Wang et al., 2018b), as shown in Figure 5A. Typically, the voltage-controlled magnetic anisotropy (VCMA) in the FM (Lee et al., 2016; Baek et al., 2018b; Wang, 2018; Grimaldi et al., 2020) (i.e., Figure 5B), as well as the gate-voltage tunable spin-orbit current from either a metal oxide (Mishra et al., 2019) as illustrated in Figure 5C, semiconductor (Chen et al., 2018b), a van der Waals crystal (Benitez et al., 2020), or a topological insulator (Fan et al., 2016), provides a class of powerful electrical manipulation methods for programmable spin-orbit logics. Besides, introducing other multiferroic behaviors beyond the ferromagnetism, such as the ferroelectric/HM/FM heterostructure (Cai et al., 2017; Belopolski et al., 2019; Filianina et al., 2020; Noël et al., 2020; Fang et al., 2020) (see Figure 5D) and the novel proposal of magnetoelectric spin-orbit logics (MESO, see Figure 5E), can also bring additional nonvolatile freedoms for realizing all electrically programmable functionalities (Manipatruni et al., 2019). Most recently, the programmable spin-orbit domain-wall logics have been demonstrated and drawing attention by controlling either the initial domain states (Lee et al., 2018) or the chirality of the domain walls (Luo et al., 2019a, 2020), as shown in Figure 5F. To look forward, more diverse methods might be proposed for the programmable spin-orbitronics, whose overall energy efficiency, scalability, and industrial feasibility should be compared and assessed before any potential practical applications.

Spin-Orbitronics in Exotic Magnetic Materials with New Physics

Although the spin-orbitronic researches were first initiated and extensively performed in FM-based materials, they have been extended to several exotic magnetic materials with new investigating of SOC physics.

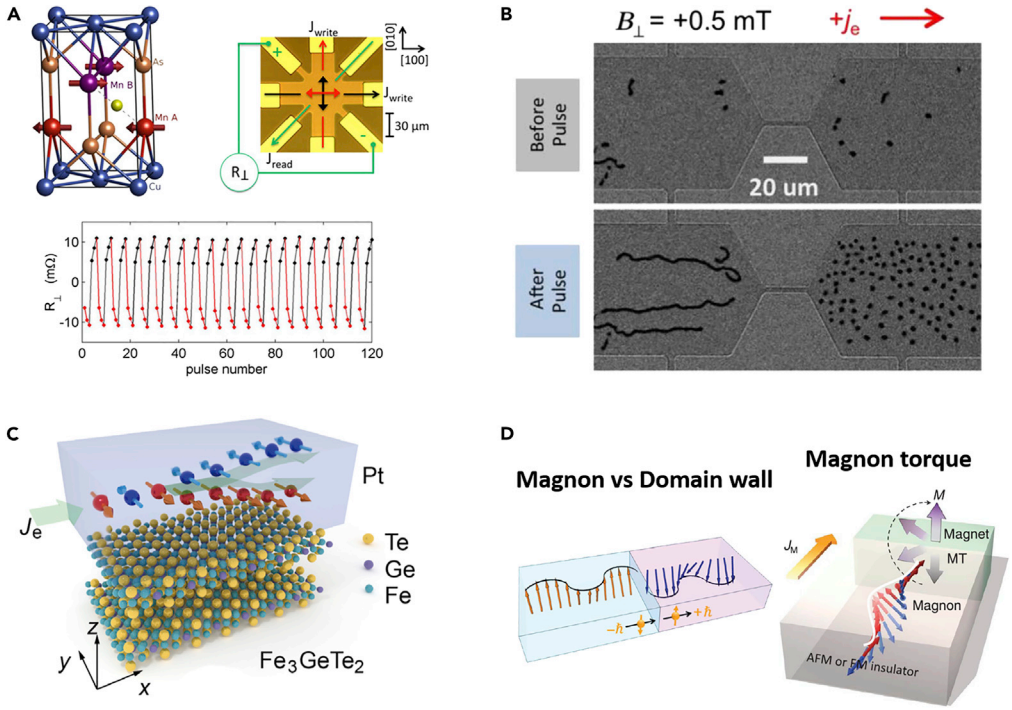

Figure 6. Representative Reprinted Works Reported on Spin-Orbitronics in Exotic Magnetic Materials beyond the Ferromagnets

(A) Electric switching of antiferromagnet. Unlike conventional SOTs generated in HM/FM bilayers, the opposite signs of spin polarization at individual spin sublattices give staggered SOTs in a single CuMnAs layer (Wadley et al., 2016).

(B) Generation and motion of magnetic skyrmions by spatially divergent SOTs (Jiang et al., 2015).

(C) Electrical switching of a Fe_3GeTe_2 van der Waals material via SOTs generated from the capping Pt layer (Wang et al., 2019a).

(D) Magnetic domain wall motions as well as magnetization switching induced by the torques mediated by spin waves (magnons), the phase and magnitude of which can also be tuned by the domain walls mutually in a nonvolatile manner (Han et al., 2019; Wang et al., 2019b).

As shown in Figure 6A, for example, the staggered SOT-induced switching of unique antiferromagnets (e.g., CuMnAs and Mn_2Au) with broken inversion symmetry in two spin-sublattices has offered an alternative solution to the writing problems for the external magnetic field-insensitive AFMs (Železný et al., 2014; Chen et al., 2019b; Wadley et al., 2016). Similarly, the sawtooth-shaped current-induced switching phenomena were also reported in HM/AFM or AFM/HM stacks of NiO/Pt, Ta/MnN/Pt, α-Fe_2O_3/Pt, and Pt/PtMn, although the mechanisms of SOT-induced switching of the Néel vectors in these systems are still debated (Baldrati et al., 2019; Zhang et al., 2019a; Chiang et al., 2019; Shi et al., 2020). Meanwhile, SOT-induced switching of other AFM coupled systems, such as the synthetic AFMs with two antiferromagnetic coupled FM layers (Shi et al., 2017; Zhang et al., 2018; Yu et al., 2018; Kong et al., 2018; Bi et al., 2017), and the compensated ferrimagnet comprising transition metal (Fe, Co, Ni) and rare earth elements (Gd, Tb, Dy, Rh, etc.) (Finley and Liu, 2016; Mishra et al., 2017; Yu et al., 2019; Pham et al., 2018; Kim et al., 2017; Han et al., 2017; An et al., 2018b; Cai et al., 2020) provide alternative approaches toward the AFM spin-orbitronics with advantages in processing speed (much higher precession frequency than FMs), data scalability (no stray field), and information security (zero net magnetization, and insensitive to external magnetic field). To date, the SOT-induced manipulation of skyrmions motion (Jiang et al., 2015; Buttner et al., 2017; Yu et al., 2016) (the topological spin textures stabilized by Dzyaloshinskii-Moriya interactions, DMI, see Figure 6B) and magnetization switching in magnetic insulators (Avci et al., 2017; Shao et al., 2018), ferromagnetic topological insulators (Fan et al., 2014b, 2016), antiferromagnetic Weyl semimetals (Tsai et al., 2020), and 2D ferromagnets (Wang et al., 2019a; Alghamdi et al., 2019; Ostwal et al., 2020) (see Figure 6C) have already been studied intensively, and it is believed that extensive investigations of SOTs in other exotic magnetic materials, such as ferromagnetic Weyl semimetals (Liu et al., 2019b; Morali et al., 2019; Belopolski

et al., 2019) and antiferromagnetic topological insulator (Guin et al., 2019; Ghosh and Manchon, 2017; Otrokov et al., 2019) could attract intriguing interests to enrich the understanding of fundamental SOC physics and corresponding potential applications. Note that the giant amplitude of inverse and direct Rashba-Edelstein effect in oxide heterostructures of $SrTiO_3$ and $LaAlO_3/SrTiO_3$ formed quasi 2D electron gas (2DEG) system also provide significant charge-spin interconversions (Noël et al., 2020), holding the promise to pave the way from oxide spin-orbitronics prospect toward low-power electrical control of magnetizations. In addition, the frontier researches on spin-orbitronics could inspire innovations in other spintronic devices, e.g., the newly reported optical spin-orbit torque (OSOT) devices with an optical means for magnetization manipulation in FM layer (Choi et al., 2020), and the magnonic devices where significant discoveries in the detection and the manipulation (see Figure 6D) of magnetization via spin waves have been recently presented (Han et al., 2019; Wang et al., 2019b; Liu et al., 2019a).

CONCLUSIONS

In summary, the latest SOT research advancements have fueled fundamental spin-orbitronic exploration and associated technical innovations. The spin-orbitronic devices based on SOT-induced magnetization switching demonstrate great advantages in terms of nonvolatility, fast processing speed, high energy efficiency, reliable endurance, potential multilevel storage, stochastic switching, and reconfigurable switching, making them promising candidates for emerging applications in processing in-memory, neuromorphic computing, probabilistic computing, avionics, and internet of things. Look toward spin-orbitronic devices development, realizing field-free SOT-induced magnetization switching in a scalable way, enhancing energy efficiency via materials engineering and implementing application with practical integration remain as major challenges to be addressed. Nevertheless, new opportunities in the 3D spin-orbitronic devices, the programmable logics, and the novel SOT research findings in exotic magnetic materials to enrich SOC physics are drawing great interests from both scientific and industrial perspectives, paving the way for more ambitious and futuristic applications of spin-orbitronic devices.

ACKNOWLEDGMENTS

The authors are grateful for the financial support from National Key R&D Program of China (Grant No. 2017YFB0405700 and 2019FYB2205100), NSFC (Grant No. 11474272 and 61774144), Chinese Academy of Sciences (Grant No. QYZDY-SSW-JSC020, XDB44000000, XDB28000000, E0YR063004 and E0SR023002), and Beijing Natural Science Foundation Key Program (Grant No. Z190007).

AUTHOR CONTRIBUTIONS

K.W. conceived the idea. Y.C. and G.X. contributed equally to this work. Y.C., G.X., and K.W. wrote the manuscript. All authors discussed and modified the manuscript.

REFERENCES

Aggarwal, S., Almasi, H., Deherrera, M., Hughes, B., Ikegawa, S., Janesky, J., Lee, H., Lu, H., Mancoff, F., Nagel, K., et al. (2019). Demonstration of a Reliable 1 Gb Standalone Spin-Transfer Torque Mram for Industrial Applications. In IEEE International Electron Devices Meeting (IEDM) (IEEE), pp. 2.1.1–2.1.4.

Akyol, M., Yu, G., Alzate, J.G., Upadhyaya, P., Li, X., Wong, K.L., Ekicibil, A., Khalili Amiri, P., and Wang, K.L. (2015). Current-induced spin-orbit torque switching of perpendicularly magnetized Hf/CoFeB/MgO and Hf/CoFeB/TaOx structures. Appl. Phys. Lett. *106*, 162409.

Alghamdi, M., Lohmann, M., Li, J., Jothi, P.R., Shao, Q., Aldosary, M., Su, T., Fokwa, B.P., and Shi, J. (2019). Highly efficient spin–orbit torque and switching of layered ferromagnet Fe_3GeTe_2. Nano Lett. *19*, 4400–4405.

Althammer, M., Meyer, S., Nakayama, H., Schreier, M., Altmannshofer, S., Weiler, M., Huebl, H., Geprägs, S., Opel, M., Gross, R., et al. (2013). Quantitative study of the spin Hall magnetoresistance in ferromagnetic insulator/normal metal hybrids. Phys. Rev. B *87*, 224401.

Amin, V.P., Li, J., Stiles, M.D., and Haney, P.M. (2019). Intrinsic spin currents in ferromagnets. Phys. Rev. B *99*, 220405.

An, H., Kageyama, Y., Kanno, Y., Enishi, N., and Ando, K. (2016). Spin-torque generator engineered by natural oxidation of Cu. Nat. Commun. *7*, 13069.

An, H., Kanno, Y., Asami, A., and Ando, K. (2018a). Giant spin-torque generation by heavily oxidized Pt. Phys. Rev. B *98*, 014401.

An, H., Ohno, T., Kanno, Y., Kageyama, Y., Monnai, Y., Maki, H., Shi, J., and Ando, K. (2018b). Current-induced magnetization switching using an electrically insulating spin-torque generator. Sci. Adv. *4*, eaar2250.

Avci, C.O., Quindeau, A., Pai, C.-F., Mann, M., Caretta, L., Tang, A.S., Onbasli, M.C., Ross, C.A., and Beach, G.S. (2017). Current-induced switching in a magnetic insulator. Nat. Mater. *16*, 309–314.

Azam, M.A., Bhattacharya, D., Querlioz, D., Ross, C.A., and Atulasimha, J. (2020). Voltage control of domain walls in magnetic nanowires for energy-efficient neuromorphic devices. Nanotechnology *31*, 145201.

Baek, S.-H.C., Amin, V.P., Oh, Y.-W., Go, G., Lee, S.-J., Lee, G.-H., Kim, K.-J., Stiles, M.D., Park, B.-G., and Lee, K.-J. (2018a). Spin currents and spin–orbit torques in ferromagnetic trilayers. Nat. Mater. *17*, 509–513.

Baek, S.-H.C., Park, K.-W., Kil, D.-S., Jang, Y., Park, J., Lee, K.-J., and Park, B.-G. (2018b). Complementary logic operation based on electric-field controlled spin–orbit torques. Nat. Electron. *1*, 398–403.

Baibich, M.N., Broto, J.M., Fert, A., Nguyen Van Dau, F., Petroff, F., Etienne, P., Creuzet, G., Friederich, A., and Chazelas, J. (1988). Giant magnetoresistance of (001)Fe/(001)Cr magnetic superlattices. Phys. Rev. Lett. *61*, 2472–2475.

Baldrati, L., Gomonay, O., Ross, A., Filianina, M., Lebrun, R., Ramos, R., Leveille, C., Fuhrmann, F., Forrest, T., Maccherozzi, F., et al. (2019). Mechanism of Néel order switching in antiferromagnetic thin films revealed by magnetotransport and direct imaging. Phys. Rev. Lett. *123*, 177201.

Baumgartner, M., Garello, K., Mendil, J., Avci, C.O., Grimaldi, E., Murer, C., Feng, J., Gabureac, M., Stamm, C., Acremann, Y., et al. (2017). Spatially and time-resolved magnetization dynamics driven by spin–orbit torques. Nat. Nanotechnol. *12*, 980–986.

Bekele, Z.A., Lan, X., Meng, K., and Liu, X. (2020). Enhanced field-free current-induced magnetization switching by interlayer exchange coupling with insulating spacer layer. J. Appl. Phys. *127*, 113902.

Bekele, Z.A., Meng, K., Miao, J., Xu, X., and Jiang, Y. (2018). Modulated spin orbit torque via controlling the oxidation level of Ti in Pt/Co/TiO_x heterostructures. Solid State Commun. *284*, 5–10.

Belopolski, I., Manna, K., Sanchez, D.S., Chang, G.Q., Ernst, B., Yin, J.X., Zhang, S.S., Cochran, T., Shumiya, N., Zheng, H., et al. (2019). Discovery of topological Weyl fermion lines and drumhead surface states in a room temperature magnet. Science *365*, 1278–1281.

Benitez, L.A., Savero Torres, W., Sierra, J.F., Timmermans, M., Garcia, J.H., Roche, S., Costache, M.V., and Valenzuela, S.O. (2020). Tunable room-temperature spin galvanic and spin Hall effects in van der Waals heterostructures. Nat. Mater. *19*, 170–175.

Berger, L. (2008). Emission of spin waves by a magnetic multilayer traversed by a current. Phys. Rev. B *54*, 9353.

Bi, C., Almasi, H., Price, K., Newhouse-Illige, T., Xu, M., Allen, S.R., Fan, X., and Wang, W. (2017). Anomalous spin-orbit torque switching in synthetic antiferromagnets. Phys. Rev. B *95*, 104434.

Binasch, G., Grunberg, P., Saurenbach, F., and Zinn, W. (1989). Enhanced magnetoresistance in layered magnetic structures with antiferromagnetic interlayer exchange. Phys. Rev. B *39*, 4828–4830.

Bishnoi, R., Ebrahimi, M., Oboril, F., and Tahoori, M.B. (2014). Architectural Aspects in Design and Analysis of SOT-Based Memories. In 2014 19th Asia and South Pacific Design Automation Conference (ASP-DAC), Singapore (IEEE), pp. 700–707.

Boehnke, A., Martens, U., Sterwerf, C., Niesen, A., Huebner, T., Von Der Ehe, M., Meinert, M., Kuschel, T., Thomas, A., and Heiliger, C. (2017). Large magneto-Seebeck effect in magnetic tunnel junctions with half-metallic Heusler electrodes. Nat. Commun. *8*, 1626.

Borders, W.A., Akima, H., Fukami, S., Moriya, S., Kurihara, S., Horio, Y., Sato, S., and Ohno, H. (2016). Analogue spin–orbit torque device for artificial-neural-network-based associative memory operation. Appl. Phys. Express *10*, 013007.

Borders, W.A., Pervaiz, A.Z., Fukami, S., Camsari, K.Y., Ohno, H., and Datta, S. (2019). Integer factorization using stochastic magnetic tunnel junctions. Nature *573*, 390–393.

Brataas, A., Kent, A.D., and Ohno, H. (2012). Current-induced torques in magnetic materials. Nat. Mater. *11*, 372–381.

Buttner, F., Lemesh, I., Schneider, M., Pfau, B., Gunther, C.M., Hessing, P., Geilhufe, J., Caretta, L., Engel, D., Kruger, B., et al. (2017). Field-free deterministic ultrafast creation of magnetic skyrmions by spin-orbit torques. Nat. Nanotechnol. *12*, 1040–1044.

Cai, K., Yang, M., Ju, H., Wang, S., Ji, Y., Li, B., Edmonds, K.W., Sheng, Y., Zhang, B., Zhang, N., et al. (2017). Electric field control of deterministic current-induced magnetization switching in a hybrid ferromagnetic/ferroelectric structure. Nat. Mater. *16*, 712–716.

Cai, K., Zhu, Z., Lee, J.M., Mishra, R., Ren, L., Pollard, S.D., He, P., Liang, G., Teo, K.L., and Yang, H. (2020). Ultrafast and energy-efficient spin–orbit torque switching in compensated ferrimagnets. Nat. Electron. *3*, 37–42.

Camsari, K.Y., Faria, R., Sutton, B.M., and Datta, S. (2017). Stochastic p-bits for invertible logic. Phys. Rev. X *7*, 031014.

Cao, Y., Rushforth, A., Sheng, Y., Zheng, H., and Wang, K. (2019). Tuning a binary ferromagnet into a multistate synapse with spinnd ene-torque-induced plasticity. Adv. Funct. Mater. *29*, 1808104.

Cao, Y., Sheng, Y., Edmonds, K.W., Ji, Y., Zheng, H., and Wang, K. (2020). Deterministic magnetization switching using lateral spin–orbit torque. Adv. Mater. *32*, 1907929.

Chandrasekaran, N. (2013). Challenges in 3D Memory Manufacturing and Process Integration. In IEEE International Electron Devices Meeting (IEDM), Washington, DC, USA, 2013, *13*IEEE International Electron Devices Meeting (IEDM), Washington, DC, USA, 2013 (IEEE), pp. 1.1–13.1.5.

Chanthbouala, A., Garcia, V., Cherifi, R.O., Bouzehouane, K., Fusil, S., Moya, X., Xavier, S., Yamada, H., Deranlot, C., Mathur, N.D., et al. (2012). A ferroelectric memristor. Nat. Mater. *11*, 860–864.

Chen, H., Zhang, S., Xu, N., Song, M., Li, X., Li, R., Zeng, Y., Hong, J., and You, L. (2018a). Binary and ternary true random number generators based on spin orbit torque. In IEEE International Electron Devices Meeting (IEDM), San Francisco, CA, USA, *36*IEEE International Electron Devices Meeting (IEDM), San Francisco, CA, USA (IEEE), pp. 5.1–36.5.4.

Chen, L., Decker, M., Kronseder, M., Islinger, R., Gmitra, M., Schuh, D., Bougeard, D., Fabian, J., Weiss, D., and Back, C.H. (2016). Robust spin-orbit torque and spin-galvanic effect at the Fe/GaAs (001) interface at room temperature. Nat. Commun. *7*, 13802.

Chen, L., Gmitra, M., Vogel, M., Islinger, R., Kronseder, M., Schuh, D., Bougeard, D., Fabian, J., Weiss, D., and Back, C.H. (2018b). Electric-field control of interfacial spin-orbit fields. Nat. Electron. *1*, 350–355.

Chen, S., Yu, J., Xie, Q., Zhang, X., Lin, W., Liu, L., Zhou, J., Shu, X., Guo, R., Zhang, Z., et al. (2019a). Free field electric switching of perpendicularly magnetized thin film by spin current gradient. ACS Appl. Mater. Inter. *11*, 30446–30452.

Chen, T.-Y., Chan, H.-I., Liao, W.-B., and Pai, C.-F. (2018c). Current-induced spin-orbit torque and field-free switching in Mo-based magnetic heterostructures. Phys. Rev. Appl. *10*, 044038.

Chen, T.-Y., Liao, W.-B., Chen, T.-Y., Tsai, T.-Y., Peng, C.-W., and Pai, C.-F. (2020a). Current-induced spin–orbit torque efficiencies in W/Pt/Co/Pt heterostructures. Appl. Phys. Lett. *116*, 072405.

Chen, T.-Y., Peng, C.-W., Tsai, T.-Y., Liao, W.-B., Wu, C.-T., Yen, H.-W., and Pai, C.-F. (2020b). Efficient spin–orbit torque switching with nonepitaxial chalcogenide heterostructures. ACS Appl. Mater. Inter. *12*, 7788–7794.

Chen, X., Kang, W., Zhu, D., Zhang, X., Lei, N., Zhang, Y., Zhou, Y., and Zhao, W. (2018d). A compact skyrmionic leaky–integrate–fire spiking neuron device. Nanoscale *10*, 6139–6146.

Chen, X., Zhou, X., Cheng, R., Song, C., Zhang, J., Wu, Y., Ba, Y., Li, H., Sun, Y., and You, Y. (2019b). Electric field control of Néel spin–orbit torque in an antiferromagnet. Nat. Mater. *18*, 931–935.

Chiang, C., Huang, S., Qu, D., Wu, P., and Chien, C. (2019). Absence of evidence of electrical switching of the antiferromagnetic Néel vector. Phys. Rev. Lett. *123*, 227203.

Choi, G.-M., Oh, J.H., Lee, D.-K., Lee, S.-W., Kim, K.W., Lim, M., Min, B.-C., Lee, K.-J., and Lee, H.-W. (2020). Optical spin-orbit torque in heavy metal-ferromagnet heterostructures. Nat. Commun. *11*, 1482.

Choi, J.-G., Lee, J.W., and Park, B.-G. (2017). Spin Hall magnetoresistance in heavy-metal/metallic-ferromagnet multilayer structures. Phys. Rev. B *96*, 174412.

Chowdhury, S., Datta, S., and Camsari, K.Y. (2019). A Probabilistic Approach to Quantum Inspired Algorithms. In IEEE International Electron Devices Meeting (IEDM), San Francisco, CA, USA (IEEE), pp. 37.5.1–37.5.4.

De La Venta, J., Wang, S., Ramirez, J., and Schuller, I.K. (2013). Control of magnetism across metal to insulator transitions. Appl. Phys. Lett. *102*, 122404.

Debashis, P., Faria, R., Camsari, K.Y., Datta, S., and Chen, Z. (2020). Correlated fluctuations in spin orbit torque coupled perpendicular nanomagnets. Phys. Rev. B *101*, 094405.

Demasius, K.U., Phung, T., Zhang, W., Hughes, B.P., Yang, S.H., Kellock, A., Han, W., Pushp, A., and Parkin, S.S.P. (2016). Enhanced spin-orbit torques by oxygen incorporation in tungsten films. Nat. Commun. *7*, 10644.

Diep, V.Q., Sutton, B., Behin-Aein, B., and Datta, S. (2014). Spin switches for compact implementation of neuron and synapse. Appl. Phys. Lett. *104*, 222405.

Djayaprawira, D.D., Tsunekawa, K., Nagai, M., Maehara, H., Yamagata, S., Watanabe, N., Yuasa, S., Suzuki, Y., and Ando, K. (2005). 230% room-

temperature magnetoresistance in CoFeB/MgO/CoFeB magnetic tunnel junctions. Appl. Phys. Lett. *86*, 092502.

Edelstein, V.M. (1990). Spin polarization of conduction electrons induced by electric current in two-dimensional asymmetric electron systems. Solid State Commun. *73*, 233–235.

Emori, S., Bauer, U., Ahn, S.-M., Martinez, E., and Beach, G.S. (2013). Current-driven dynamics of chiral ferromagnetic domain walls. Nat. Mater. *12*, 611–616.

Fan, X., Celik, H., Wu, J., Ni, C., Lee, K.-J., Lorenz, V.O., and Xiao, J.Q. (2014a). Quantifying interface and bulk contributions to spin–orbit torque in magnetic bilayers. Nat. Commun. *5*, 3042.

Fan, Y., Kou, X., Upadhyaya, P., Shao, Q., Pan, L., Lang, M., Che, X., Tang, J., Montazeri, M., Murata, K., et al. (2016). Electric-field control of spin–orbit torque in a magnetically doped topological insulator. Nat. Nanotechnol. *11*, 352–359.

Fan, Y., Upadhyaya, P., Kou, X., Lang, M., Takei, S., Wang, Z., Tang, J., He, L., Chang, L.-T., Montazeri, M., et al. (2014b). Magnetization switching through giant spin–orbit torque in a magnetically doped topological insulator heterostructure. Nat. Mater. *13*, 699–704.

Fang, M., Wang, Y., Wang, H., Hou, Y., Vetter, E., Kou, Y., Yang, W., Yin, L., Xiao, Z., Li, Z., et al. (2020). Tuning the interfacial spin-orbit coupling with ferroelectricity. Nat. Commun. *11*, 2627.

Farkhani, H., Böhnert, T., Tarequzzaman, M., Costa, J.D., Jenkins, A., Ferreira, R., Madsen, J.K., and Moradi, F. (2019). Lao-NCS: laser assisted spin torque nano oscillator-based neuromorphic computing system. Front. Neurosci. *13*, 1429.

Filianina, M., Hanke, J.-P., Lee, K., Han, D.-S., Jaiswal, S., Rajan, A., Jakob, G., Mokrousov, Y., and Kläui, M. (2020). Electric-field control of spin-orbit torques in perpendicularly magnetized W/CoFeB/MgO films. Phys. Rev. Lett. *124*, 217701.

Finley, J., and Liu, L. (2016). Spin-orbit-torque efficiency in compensated ferrimagnetic cobalt-terbium alloys. Phys. Rev. Appl. *6*, 054001.

Finocchio, G., Moriyama, T., De Rose, R., Siracusano, G., Lanuzza, M., Puliafito, V., Chiappini, S., Crupi, F., Zeng, Z., and Ono, T. (2019). Spin-orbit torque based physical unclonable function. arXiv. arXiv:1910.12464.

Friesen, C., Osterhage, H., Friedlein, J., Schlenhoff, A., Wiesendanger, R., and Krause, S. (2019). Magneto-Seebeck tunneling on the atomic scale. Science *363*, 1065–1067.

Fukami, S., Zhang, C., Duttagupta, S., Kurenkov, A., and Ohno, H. (2016). Magnetization switching by spin-orbit torque in an antiferromagnet-ferromagnet bilayer system. Nat. Mater. *15*, 535–541.

Fulara, H., Zahedinejad, M., Khymyn, R., Awad, A., Muralidhar, S., Dvornik, M., and Åkerman, J. (2019). Spin-orbit torque–driven propagating spin waves. Sci. Adv. *5*, eaax8467.

Ganguly, A., Kondou, K., Sukegawa, H., Mitani, S., Kasai, S., Niimi, Y., Otani, Y., and Barman, A. (2014). Thickness dependence of spin torque ferromagnetic resonance in $Co_{75}Fe_{25}$/Pt bilayer films. Appl. Phys. Lett. *104*, 072405.

Gao, Y., Al-Sarawi, S.F., and Abbott, D. (2020). Physical unclonable functions. Nat. Electron. *3*, 81–91.

Garello, K., Yasin, F., Hody, H., Couet, S., Souriau, L., Sharifi, S., Swerts, J., Carpenter, R., Rao, S., Kim, W., et al. (2019a). Manufacturable 300mm Platform Solution for Field-free Switching SOT-MRAM. 2019 Symposium on VLSI Circuits, Kyoto, Japan, 9-14 June, 2019a (IEEE), pp. T194–T195.

Garello, K., Yasin, F., and Kar, G.S. (2019b). Spin-Orbit Torque MRAM for ultrafast embedded memories: from fundamentals to large scale technology integration. In IEEE 11th International Memory Workshop (IMW), Monterey, CA, USA, 2019 (IEEE). https://doi.org/10.1109/IMW.2019.8739466.

Ghosh, S., and Manchon, A. (2017). Spin-orbit torque in two-dimensional antiferromagnetic topological insulators. Phys. Rev. B *95*, 035422.

Gidon, A., Zolnik, T.A., Fidzinski, P., Bolduan, F., Papoutsi, A., Poirazi, P., Holtkamp, M., Vida, I., and Larkum, M.E. (2020). Dendritic action potentials and computation in human layer 2/3 cortical neurons. Science *367*, 83–87.

Greenemeier, L. (2008). Japanese Satellite First to Use Magnetic Memory. https://www.scientificamerican.com/article/japanese-satellite-mram-freescale/.

Grimaldi, E., Krizakova, V., Sala, G., Yasin, F., Couet, S., Kar, G.S., Garello, K., and Gambardella, P. (2020). Single-shot dynamics of spin–orbit torque and spin transfer torque switching in three-terminal magnetic tunnel junctions. Nat. Nanotechnol. *15*, 111–117.

Grollier, J., Querlioz, D., Camsari, K., Everschor-Sitte, K., Fukami, S., and Stiles, M. (2020). Neuromorphic spintronics. Nat. Electron. *31*, 092001.

Guin, S.N., Vir, P., Zhang, Y., Kumar, N., Watzman, S.J., Fu, C., Liu, E., Manna, K., Schnelle, W., Gooth, J., et al. (2019). Zero-field nernst effect in a ferromagnetic kagome-lattice weyl-semimetal $Co_3Sn_2S_2$. Adv. Mater. *31*, 1806622.

Han, J., Richardella, A., Siddiqui, S.A., Finley, J., Samarth, N., and Liu, L. (2017). Room-temperature spin-orbit torque switching induced by a topological insulator. Phys. Rev. Lett. *119*, 077702.

Han, J.H., Zhang, P.X., Hou, J.T., Siddiqui, S.A., and Liu, L.Q. (2019). Mutual control of coherent spin waves and magnetic domain walls in a magnonic device. Science *366*, 1121–1125.

Hao, Q., and Xiao, G. (2015). Giant spin Hall effect and switching induced by spin-transfer torque in a $W/Co_{40}Fe_{40}B_{20}/MgO$ structure with perpendicular magnetic anisotropy. Phys. Rev. Appl. *3*, 034009.

He, Z., Zhang, Y., Angizi, S., Gong, B., and Fan, D. (2018). Exploring a sot-mram based in-memory computing for data processing. IEEE Trans. Multi-Scale Comput. Syst. *4*, 676–685.

Hong, J., Stone, M., Navarrete, B., Luongo, K., Zheng, Q., Yuan, Z., Xia, K., Xu, N., Bokor, J., You, L., et al. (2018). 3D multilevel spin transfer torque devices. Appl. Phys. Lett. *112*, 112402.

Hu, C., Zhang, D., Yan, F., Li, Y., Lv, Q., Zhu, W., Wei, Z., Chang, K., and Wang, K. (2020). From two- to multi-state vertical spin valves without spacer layer based on Fe_3GeTe_2 van der Waals homo-junctions. Sci. Bull. *65*, 1072–1077.

Huai, Y., Yang, H., Hao, X., Wang, Z., Malmhall, R., Sato, K., Zhang, J., Jung, D.H., Wang, X., Xu, P., et al. (2018). High density 3D cross-point STT-MRAM. In IEEE International Memory Workshop (IMW), Kyoto, Japan, 2018 (IEEE). https://doi.org/10.1109/IMW.2018.8388833.

Huang, K.-F., Wang, D.-S., Lin, H.-H., and Lai, C.-H. (2015). Engineering spin-orbit torque in Co/Pt multilayers with perpendicular magnetic anisotropy. Appl. Phys. Lett. *107*, 232407.

Hughes, H., Bussmann, K., Mcmarr, P.J., Cheng, S.-F., Shull, R., Chen, A.P., Schafer, S., Mewes, T., Ong, A., Chen, E., et al. (2012). Radiation studies of spin-transfer torque materials and devices. IEEE Trans. Nucl. Sci. *59*, 3027–3033.

Ielmini, D., and Wong, H.-S.P. (2018). In-memory computing with resistive switching devices. Nat. Electron. *1*, 333–343.

Ignatov, M., Ziegler, M., Hansen, M., and Kohlstedt, H. (2017). Memristive stochastic plasticity enables mimicking of neural synchrony: memristive circuit emulates an optical illusion. Sci. Adv. *3*, e1700849.

Ikeda, S., Hayakawa, J., Ashizawa, Y., Lee, Y., Miura, K., Hasegawa, H., Tsunoda, M., Matsukura, F., and Ohno, H. (2008). Tunnel magnetoresistance of 604% at 300 K by suppression of Ta diffusion in CoFeB/MgO/CoFeB pseudo-spin-valves annealed at high temperature. Appl. Phys. Lett. *93*, 082508.

Jiang, W., Upadhyaya, P., Zhang, W., Yu, G., Jungfleisch, M.B., Fradin, F.Y., Pearson, J.E., Tserkovnyak, Y., Wang, K.L., Heinonen, O., et al. (2015). Blowing magnetic skyrmion bubbles. Science *349*, 283–286.

Jo, S.H., Chang, T., Ebong, I., Bhadviya, B.B., Mazumder, P., and Lu, W. (2010). Nanoscale memristor device as synapse in neuromorphic systems. Nano Lett. *10*, 1297–1301.

Kampfrath, T., Battiato, M., Maldonado, P., Eilers, G., Nötzold, J., Mährlein, S., Zbarsky, V., Freimuth, F., Mokrousov, Y., Blügel, S., et al. (2013). Terahertz spin current pulses controlled by magnetic heterostructures. Nat. Nanotechnol. *8*, 256–260.

Khang, N.H.D., Ueda, Y., and Hai, P.N. (2018). A conductive topological insulator with large spin Hall effect for ultralow power spin–orbit torque switching. Nat. Mater. *17*, 808–813.

Kim, K.-J., Kim, S.K., Hirata, Y., Oh, S.-H., Tono, T., Kim, D.-H., Okuno, T., Ham, W.S., Kim, S., Go, G., et al. (2017). Fast domain wall motion in the vicinity of the angular momentum compensation temperature of ferrimagnets. Nat. Mater. *16*, 1187–1192.

Kim, Y., Fong, X., and Roy, K. (2015). Spin-orbit-torque-based spin-dice: a true random-number generator. IEEE Magn. Lett. *6*, 3001004.

Kimura, T., Otani, Y., Sato, T., Takahashi, S., and Maekawa, S. (2007). Room-temperature reversible spin Hall effect. Phys. Rev. Lett. *98*, 156601.

Kiselev, S.I., Sankey, J., Krivorotov, I., Emley, N., Schoelkopf, R., Buhrman, R., and Ralph, D. (2003). Microwave oscillations of a nanomagnet driven by a spin-polarized current. Nature *425*, 380–383.

Kobayashi, D., Kakehashi, Y., Hirose, K., Onoda, S., Makino, T., Ohshima, T., Ikeda, S., Yamanouchi, M., Sato, H., Enobio, E.C., et al. (2014). Influence of heavy ion irradiation on perpendicular-anisotropy CoFeB-MgO magnetic tunnel junctions. IEEE Trans. Nucl. Sci. *61*, 1710–1716.

Kondou, K., Sukegawa, H., Mitani, S., Tsukagoshi, K., and Kasai, S. (2012). Evaluation of spin Hall angle and spin diffusion length by using spin current-induced ferromagnetic resonance. Appl. Phys. Express *5*, 073002.

Kong, W., Wan, C., Tao, B., Fang, C., Huang, L., Guo, C., Irfan, M., and Han, X. (2018). Study of spin-orbit torque induced magnetization switching in synthetic antiferromagnet with ultrathin Ta spacer layer. Appl. Phys. Lett. *113*, 162402.

Kong, W.J., Wan, C.H., Wang, X., Tao, B.S., Huang, L., Fang, C., Guo, C.Y., Guang, Y., Irfan, M., and Han, X.F. (2019). Spin–orbit torque switching in a T-type magnetic configuration with current orthogonal to easy axes. Nat. Commun. *10*, 233.

Kurenkov, A., Duttagupta, S., Zhang, C., Fukami, S., Horio, Y., and Ohno, H. (2019). Artificial neuron and synapse realized in an antiferromagnet/ferromagnet heterostructure using dynamics of spin–orbit torque switching. Adv. Mater. *31*, 1900636.

Kurenkov, A., Zhang, C., Duttagupta, S., Fukami, S., and Ohno, H. (2017). Device-size dependence of field-free spin-orbit torque induced magnetization switching in antiferromagnet/ferromagnet structures. Appl. Phys. Lett. *110*, 092410.

Kuzum, D., Jeyasingh, R.G., Lee, B., and Wong, H.-S.P. (2012). Nanoelectronic programmable synapses based on phase change materials for brain-inspired computing. Nano Lett. *12*, 2179–2186.

Lau, Y.-C., Betto, D., Rode, K., Coey, J.M.D., and Stamenov, P. (2016). Spin–orbit torque switching without an external field using interlayer exchange coupling. Nat. Nanotechnol. *11*, 758–762.

Lee, H.-Y., Kim, S., Park, J.-Y., Oh, Y.-W., Park, S.-Y., Ham, W., Kotani, Y., Nakamura, T., Suzuki, M., and Ono, T. (2019). Enhanced spin–orbit torque via interface engineering in Pt/CoFeB/MgO heterostructures. APL Mater. *7*, 031110.

Lee, H., Ebrahimi, F., Amiri, P.K., and Wang, K.L. (2016). Low-power, high-density spintronic programmable logic with voltage-gated spin Hall effect in magnetic tunnel junctions. IEEE Magn. Lett. *7*, 310205.

Lee, J.M., Cai, K., Yang, G., Liu, Y., Ramaswamy, R., He, P., and Yang, H. (2018). Field-free spin–orbit torque switching from geometrical domain-wall pinning. Nano Lett. *18*, 4669–4674.

Lee, J.W., Oh, Y.-W., Park, S.-Y., Figueroa, A.I., Van Der Laan, G., Go, G., Lee, K.-J., and Park, B.-G. (2017). Enhanced spin-orbit torque by engineering Pt resistivity in Pt/Co/Al Ox structures. Phys. Rev. B *96*, 064405.

Lee, O., You, L., Jang, J., Subramanian, V., and Salahuddin, S. (2015). Flexible spin-orbit torque devices. Appl. Phys. Lett. *107*, 252401.

Lequeux, S., Sampaio, J., Cros, V., Yakushiji, K., Fukushima, A., Matsumoto, R., Kubota, H., Yuasa, S., and Grollier, J. (2016). A magnetic synapse: multilevel spin-torque memristor with perpendicular anisotropy. Sci. Rep. *6*, 31510.

Li, Y., Edmonds, K.W., Liu, X., Zheng, H., and Wang, K. (2019). Manipulation of magnetization by spin-orbit torque. Adv. Quan. Tech. *2*, 1800052.

Li, Y., Liang, J., Yang, H., Zheng, H., and Wang, K. (2020). Current-induced out-of-plane effective magnetic field in antiferromagnet/heavy metal/ferromagnet/heavy metal multilayer. Appl. Phys. Lett. *117*, 092404.

Li, P., Wu, W., Wen, Y., Zhang, C., Zhang, J., Zhang, S., Yu, Z., Yang, S.A., Manchon, A., and Zhang, X.-X. (2018). Spin-momentum locking and spin-orbit torques in magnetic nano-heterojunctions composed of Weyl semimetal WTe_2. Nat. Commun. *9*, 3990.

Liang, X., Zhang, X., Xia, J., Ezawa, M., Zhao, Y., Zhao, G., and Zhou, Y. (2020). A spiking neuron constructed by the skyrmion-based spin torque nano-oscillator. Appl. Phys. Lett. *116*, 122402.

Liebing, N., Serrano-Guisan, S., Rott, K., Reiss, G., Langer, J., Ocker, B., and Schumacher, H. (2011). Tunneling magnetothermopower in magnetic tunnel junction nanopillars. Phys. Rev. Lett. *107*, 177201.

Liu, C., Wu, S., Zhang, J., Chen, J., Ding, J., Ma, J., Zhang, Y., Sun, Y., Tu, S., and Wang, H. (2019a). Current-controlled propagation of spin waves in antiparallel, coupled domains. Nat. Nanotechnol. *14*, 691–697.

Liu, D., Liang, A., Liu, E., Xu, Q., Li, Y., Chen, C., Pei, D., Shi, W., Mo, S., Dudin, P., et al. (2019b). Magnetic Weyl semimetal phase in a Kagomé crystal. Science *365*, 1282–1285.

Liu, J., Ohkubo, T., Mitani, S., Hono, K., and Hayashi, M. (2015). Correlation between the spin Hall angle and the structural phases of early 5d transition metals. Appl. Phys. Lett. *107*, 232408.

Liu, L., Moriyama, T., Ralph, D., and Buhrman, R. (2011). Spin-torque ferromagnetic resonance induced by the spin Hall effect. Phys. Rev. Lett. *106*, 036601.

Liu, L., Pai, C.-F., Li, Y., Tseng, H., Ralph, D., and Buhrman, R. (2012). Spin-torque switching with the giant spin Hall effect of tantalum. Science *336*, 555–558.

Liu, L., Qin, Q., Lin, W., Li, C., Xie, Q., He, S., Shu, X., Zhou, C., Lim, Z., Yu, J., et al. (2019c). Current-induced magnetization switching in all-oxide heterostructures. Nat. Nanotechnol. *14*, 939–944.

Liu, L., Yu, J., González-Hernández, R., Li, C., Deng, J., Lin, W., Zhou, C., Zhou, T., Zhou, J., and Wang, H. (2020a). Electrical switching of perpendicular magnetization in a single ferromagnetic layer. Phys. Rev. B *101*, 220402.

Liu, X., Lam, K.H., Zhu, K., Zheng, C., Li, X.L., Du, Y., Liu, C., and Pong, P.W.T. (2019d). Overview of spintronic sensors with internet of things for smart living. IEEE Trans. Magn. *55*, 0800222.

Liu, X.H., Edmonds, K.W., Zhou, Z.P., and Wang, K.Y. (2020b). Tuning interfacial spins in antiferromagnetic-ferromagnetic-heavy-metal heterostructures via spin-orbit torque. Phys. Rev. Appl. *13*, 014059.

Liu, Y., Wang, Z., Li, Z., Wang, X., and Zhao, W. (2018). A spin orbit torque based true random number generator with real-time optimization. In IEEE 18th International Conference on Nanotechnology (IEEE-NANO), Cork, Ireland, 2018 (IEEE). https://doi.org/10.1109/NANO.2018.8626347.

Luo, Z., Dao, T.P., Hrabec, A., Vijayakumar, J., Kleibert, A., Baumgartner, M., Kirk, E., Cui, J., Savchenko, T., Krishnaswamy, G., et al. (2019a). Chirally coupled nanomagnets. Science *363*, 1435–1439.

Luo, Z., Hrabec, A., Dao, T.P., Sala, G., Finizio, S., Feng, J., Mayr, S., Raabe, J., Gambardella, P., and Heyderman, L.J. (2020). Current-driven magnetic domain-wall logic. Nature *579*, 214–218.

Luo, Z., Zhang, Q., Xu, Y., Yang, Y., Zhang, X., and Wu, Y. (2019b). Spin-orbit torque in a single ferromagnetic layer induced by surface spin rotation. Phys. Rev. Appl. *11*, 064021.

Ma, Q., Li, Y., Gopman, D., Kabanov, Y.P., Shull, R., and Chien, C. (2018). Switching a perpendicular ferromagnetic layer by competing spin currents. Phys. Rev. Lett. *120*, 117703.

Macneill, D., Stiehl, G., Guimaraes, M., Buhrman, R., Park, J., and Ralph, D. (2017). Control of spin–orbit torques through crystal symmetry in WTe 2/ferromagnet bilayers. Nat. Phys. *13*, 300–305.

Mahendra, D., Grassi, R., Chen, J.-Y., Jamali, M., Hickey, D.R., Zhang, D., Zhao, Z., Li, H., Quarterman, P., Lv, Y., et al. (2018). Room-temperature high spin–orbit torque due to quantum confinement in sputtered $Bi_xSe_{(1-x)}$ films. Nat. Mater. *17*, 800–807.

Manchon, A., Koo, H.C., Nitta, J., Frolov, S.M., and Duine, R.A. (2015). New perspectives for Rashba spin-orbit coupling. Nat. Mater. *14*, 871–882.

Manchon, A., Železný, J., Miron, I.M., Jungwirth, T., Sinova, J., Thiaville, A., Garello, K., and Gambardella, P. (2019). Current-induced spin-orbit torques in ferromagnetic and antiferromagnetic systems. Rev. Mod. Phys. *91*, 035004.

Manipatruni, S., Nikonov, D.E., Lin, C.-C., Gosavi, T.A., Liu, H., Prasad, B., Huang, Y.-L., Bonturim, E., Ramesh, R., and Young, I.A. (2019). Scalable energy-efficient magnetoelectric spin–orbit logic. Nature *565*, 35–42.

Mcguire, T., and Potter, R. (1975). Anisotropic magnetoresistance in ferromagnetic 3d alloys. IEEE Trans. Magnetics *11*, 1018–1038.

Mendes, J., Mello, S., Santos, O.A., Cunha, R., Rodríguez-Suárez, R., Azevedo, A., and Rezende, S. (2017). Inverse spin Hall effect in the semiconductor (Ga, Mn) as at room temperature. Phys. Rev. B *95*, 214405.

Mikolajick, T., Dehm, C., Hartner, W., Kasko, I., Kastner, M., Nagel, N., Moert, M., and Mazure, C. (2001). FeRAM technology for high density applications. Microelectron. Reliab. *41*, 947–950.

Miron, I.M., Garello, K., Gaudin, G., Zermatten, P.-J., Costache, M.V., Auffret, S., Bandiera, S., Rodmacq, B., Schuhl, A., and Gambardella, P. (2011). Perpendicular switching of a single ferromagnetic layer induced by in-plane current injection. Nature *476*, 189–193.

Mishra, R., Mahfouzi, F., Kumar, D., Cai, K., Chen, M., Qiu, X., Kioussis, N., and Yang, H. (2019). Electric-field control of spin accumulation direction for spin-orbit torques. Nat. Commun. *10*, 248.

Mishra, R., Yu, J., Qiu, X., Motapothula, M., Venkatesan, T., and Yang, H. (2017). Anomalous current-induced spin torques in ferrimagnets near compensation. Phys. Rev. Lett. *118*, 167201.

Moradi, F., Farkhani, H., Zeinali, B., Ghanatian, H., Pelloux-Prayer, J.M.A., Boehnert, T., Zahedinejad, M., Heidari, H., Nabaei, V., Ferreira, R., et al. (2019). Spin-Orbit-Torque-based devices, circuits and architectures. arXiv. arXiv:1912.01347.

Morali, N., Batabyal, R., Nag, P.K., Liu, E., Xu, Q., Sun, Y., Yan, B., Felser, C., Avraham, N., and Beidenkopf, H. (2019). Fermi-arc diversity on surface terminations of the magnetic Weyl semimetal $Co_3Sn_2S_2$. Science *365*, 1286–1291.

Nakayama, H., Althammer, M., Chen, Y.T., Uchida, K., Kajiwara, Y., Kikuchi, D., Ohtani, T., Geprägs, S., Opel, M., Takahashi, S., et al. (2013). Spin Hall magnetoresistance induced by a nonequilibrium proximity effect. Phys. Rev. Lett. *110*, 206601.

Nguyen, M.-H., Ralph, D., and Buhrman, R. (2016a). Spin torque study of the spin Hall conductivity and spin diffusion length in platinum thin films with varying resistivity. Phys. Rev. Lett. *116*, 126601.

Nguyen, M.-H., Zhao, M., Ralph, D., and Buhrman, R. (2016b). Enhanced spin Hall torque efficiency in $Pt_{100-x}Al_x$ and $Pt_{100-x}Hf_x$ alloys arising from the intrinsic spin Hall effect. Appl. Phys. Lett. *108*, 242407.

Noël, P., Trier, F., Arche, L.M.V., Bréhin, J., Vaz, D.C., Garcia, V., Fusil, S., Barthélémy, A., Vila, L., Bibes, M., et al. (2020). Non-volatile electric control of spin–charge conversion in a $SrTiO_3$ Rashba system. Nature *580*, 483–486.

Oh, Y.-W., Chris Baek, S.-H., Kim, Y.M., Lee, H.Y., Lee, K.-D., Yang, C.-G., Park, E.-S., Lee, K.-S., Kim, K.-W., Go, G., et al. (2016). Field-free switching of perpendicular magnetization through spin–orbit torque in antiferromagnet/ferromagnet/oxide structures. Nat. Nanotechnol. *11*, 878–884.

Olejník, K., Schuler, V., Marti, X., Novák, V., Kašpar, Z., Wadley, P., Campion, R.P., Edmonds, K.W., Gallagher, B.L., Garces, J., et al. (2017). Antiferromagnetic CuMnAs multi-level memory cell with microelectronic compatibility. Nat. Commun. *8*, 15434.

Ostwal, V., Shen, T., and Appenzeller, J. (2020). Efficient spin-orbit torque switching of the semiconducting van der Waals ferromagnet $Cr_2Ge_2Te_6$. Adv. Mater. *32*, e1906021.

Otrokov, M.M., Klimovskikh, I.I., Bentmann, H., Estyunin, D., Zeugner, A., Aliev, Z.S., Gaß, S., Wolter, A.U.B., Koroleva, A.V., Shikin, A.M., et al. (2019). Prediction and observation of an antiferromagnetic topological insulator. Nature *576*, 416–422.

Park, J.-Y., Kim, J.-M., Ryu, J., Jeong, J., and Park, B.-G. (2019). Effects of proton and ion beam radiation on magnetic tunnel junctions. Thin Solid Films *686*, 137432.

Pham, T.H., Je, S.-G., Vallobra, P., Fache, T., Lacour, D., Malinowski, G., Cyrille, M.-C., Gaudin, G., Boulle, O., Hehn, M., et al. (2018). Thermal contribution to the spin-orbit torque in metallic-ferrimagnetic systems. Phys. Rev. Appl. *9*, 064032.

Preskill, J. (2018). Quantum computing in the NISQ era and beyond. Bull. Am. Phys. Soc. *2*, 79.

Qiu, X., Narayanapillai, K., Wu, Y., Deorani, P., Yang, D.-H., Noh, W.-S., Park, J.-H., Lee, K.-J., Lee, H.-W., and Yang, H. (2015). Spin–orbit-torque engineering via oxygen manipulation. Nat. Nanotechnol. *10*, 333.

Qiu, X., Shi, Z., Fan, W., Zhou, S., and Yang, H. (2018). Characterization and manipulation of spin orbit torque in magnetic heterostructures. Adv. Mater. *30*, 1705699.

Ramaswamy, R., Lee, J.M., Cai, K., and Yang, H. (2018). Recent advances in spin-orbit torques: moving towards device applications. Appl. Phys. Rev. *5*, 031107.

Razavi, A., Wu, H., Shao, Q., Fang, C., Dai, B., Wong, K., Han, X., Yu, G., and Wang, K.L. (2020). Deterministic spin–orbit torque switching by a light-metal insertion. Nano Lett. *20*, 3703–3709.

Ren, F., Jander, A., Dhagat, P., and Nordman, C. (2012). Radiation tolerance of magnetic tunnel junctions with MgO tunnel barriers. IEEE Trans. Nucl. Sci. *59*, 3034–3038.

Rojas-Sánchez, J.-C., Reyren, N., Laczkowski, P., Savero, W., Attané, J.-P., Deranlot, C., Jamet, M., George, J.-M., Vila, L., and Jaffrès, H. (2014). Spin pumping and inverse spin Hall effect in platinum: the essential role of spin-memory loss at metallic interfaces. Phys. Rev. Lett. *112*, 106602.

Sato, H., Honjo, H., Watanabe, T., Niwa, M., Koike, H., Miura, S., Saito, T., Inoue, H., Nasuno, T., Tanigawa, T., et al. (2018a). 14ns write speed 128Mb density Embedded STT-MRAM with endurance>1010 and 10yrs retention@85°C using novel low damage MTJ integration process. In IEEE International Electron Devices Meeting (IEDM), San Francisco, CA, USA, 2018, *27*IEEE International Electron Devices Meeting (IEDM), San Francisco, CA, USA, 2018 (IEEE), pp. 2.1–27.2.4.

Sato, N., Schultheiss, K., Korber, L., Puwenberg, N., Muhl, T., Awad, A.A., Arekapudi, S.S.P.K., Hellwig, O., Fassbender, J., and Schultheiss, H. (2019). Domain wall based spin-Hall nano-oscillators. Phys. Rev. Lett. *123*, 057204.

Sato, N., Xue, F., White, R.M., Bi, C., and Wang, S.X. (2018b). Two-terminal spin–orbit torque magnetoresistive random access memory. Nat. Electron. *1*, 508–511.

Seifert, T., Jaiswal, S., Martens, U., Hannegan, J., Braun, L., Maldonado, P., Freimuth, F., Kronenberg, A., Henrizi, J., Radu, I., et al. (2016). Efficient metallic spintronic emitters of ultrabroadband terahertz radiation. Nat. Photon. *10*, 483–488.

Sengupta, A., Al Azim, Z., Fong, X., and Roy, K. (2015a). Spin-orbit torque induced spike-timing dependent plasticity. Appl. Phys. Lett. *106*, 093704.

Sengupta, A., Choday, S.H., Kim, Y., and Roy, K. (2015b). Spin orbit torque based electronic neuron. Appl. Phys. Lett. *106*, 143701.

Sengupta, A., Parsa, M., Han, B., and Roy, K. (2016). Probabilistic deep spiking neural systems enabled by magnetic tunnel junction. IEEE Trans. Electron. Devices *63*, 2963–2970.

Shao, Q., Tang, C., Yu, G., Navabi, A., Wu, H., He, C., Li, J., Upadhyaya, P., Zhang, P., Razavi, S.A., et al. (2018). Role of dimensional crossover on spin-orbit torque efficiency in magnetic insulator thin films. Nat. Commun. *9*, 3612.

Shao, Q., Yu, G., Lan, Y.-W., Shi, Y., Li, M.-Y., Zheng, C., Zhu, X., Li, L.-J., Amiri, P.K., and Wang, K.L. (2016). Strong Rashba-Edelstein effect-induced spin–orbit torques in monolayer transition metal dichalcogenide/ferromagnet bilayers. Nano Lett. *16*, 7514–7520.

Sheng, Y., Cao, Y., Ma, X., and Wang, K. (2019). Modification of spin-obit torques using the Ta oxidation buffer layer. J. Magn. Magn. Mater. *481*, 12–15.

Sheng, Y., Edmonds, K.W., Ma, X., Zheng, H., and Wang, K. (2018a). Adjustable current-induced magnetization switching utilizing interlayer exchange coupling. Adv. Electron. Mater. *4*, 1800224.

Sheng, Y., Li, Y., Ma, X., and Wang, K. (2018b). Current-induced four-state magnetization switching by spin-orbit torques in perpendicular ferromagnetic trilayers. Appl. Phys. Lett. *113*, 112406.

Shi, G., Wan, C., Chang, Y., Li, F., Zhou, X., Zhang, P., Cai, J., Han, X., Pan, F., and Song, C. (2017). Spin-orbit torque in MgO/CoFeB/Ta/CoFeB/MgO symmetric structure with interlayer antiferromagnetic coupling. Phys. Rev. B *95*, 104435.

Shi, J., Lopez-Dominguez, V., Garesci, F., Wang, C., Almasi, H., Grayson, M., Finocchio, G., and Khalili Amiri, P. (2020). Electrical manipulation of the magnetic order in antiferromagnetic PtMn pillars. Nat. Electron. *3*, 92–98.

Shi, S., Liang, S., Zhu, Z., Cai, K., Pollard, S.D., Wang, Y., Wang, J., Wang, Q., He, P., Yu, J., et al. (2019). All-electric magnetization switching and Dzyaloshinskii–Moriya interaction in WTe_2/ferromagnet heterostructures. Nat. Nanotechnol. *14*, 945–949.

Shi, S., Ou, Y., Aradhya, S., Ralph, D., and Buhrman, R. (2018). Fast low-current spin-orbit-torque switching of magnetic tunnel junctions

through atomic modifications of the free-layer interfaces. Phys. Rev. Appl. *9*, 011002.

Shreya, S., Jain, A., and Kaushik, B.K. (2020). Computing-in-Memory architecture using energy-efficient multilevel voltage-controlled spin-orbit torque device. IEEE Trans. Electron Devices *67*, 1972–1979.

Siddiqui, S.A., Dutta, S., Tang, A., Liu, L., Ross, C.A., and Baldo, M.A. (2019). Magnetic domain wall based synaptic and activation function generator for neuromorphic accelerators. Nano Lett. *20*, 1033–1040.

Sinova, J., Valenzuela, S.O., Wunderlich, J., Back, C., and Jungwirth, T. (2015). Spin hall effects. Rev. Mod. Phys. *87*, 1213.

Slaughter, J.M., Nagel, K., Whig, R., Deshpande, S., Aggarwal, S., Deherrera, M., Janesky, J., Lin, M., Chia, H., Hossain, M., et al. (2016). Technology for reliable spin-torque MRAM products. In IEEE International Electron Devices Meeting (IEDM), San Francisco, CA, USA, 3-7 Dec 2016 (IEEE), pp. 21.5.1–21.5.4.

Slonczewski, J.C. (1996). Current-driven excitation of magnetic multilayers. J. Magn. Magn. Mater. *159*, L1.

Song, K.M., Jeong, J.-S., Pan, B., Zhang, X., Xia, J., Cha, S., Park, T.-E., Kim, K., Finizio, S., Raabe, J., et al. (2020a). Skyrmion-based artificial synapses for neuromorphic computing. Nat. Electron. *3*, 148–155.

Song, P., Hsu, C.-H., Vignale, G., Zhao, M., Liu, J., Deng, Y., Fu, W., Liu, Y., Zhang, Y., Lin, H., et al. (2020b). Coexistence of large conventional and planar spin Hall effect with long spin diffusion length in a low-symmetry semimetal at room temperature. Nat. Mater. *19*, 292–298.

Stiehl, G.M., Li, R., Gupta, V., El Baggari, I., Jiang, S., Xie, H., Kourkoutis, L.F., Mak, K.F., Shan, J., and Buhrman, R.A. (2019). Layer-dependent spin-orbit torques generated by the centrosymmetric transition metal dichalcogenide β– $MoTe_2$. Phys. Rev. B *100*, 184402.

Stoliar, P., Tranchant, J., Corraze, B., Janod, E., Besland, M.-P., Tesler, F., Rozenberg, M., and Cario, L. (2017). A leaky-integrate-and-fire neuron analog realized with a Mott insulator. Adv. Funct. Mater. *27*, 1604740.

Sutton, B., Camsari, K.Y., Behin-Aein, B., and Datta, S. (2017). Intrinsic optimization using stochastic nanomagnets. Sci. Rep. *7*, 44370.

Tang, M., Shen, K., Xu, S., Yang, H., Hu, S., Lü, W., Li, C., Li, M., Yuan, Z., and Pennycook, S.J. (2020). Bulk spin torque-driven perpendicular magnetization switching in L10 FePt single layer. Adv. Mater. *32*, 2002607.

Tao, X., Liu, Q., Miao, B., Yu, R., Feng, Z., Sun, L., You, B., Du, J., Chen, K., Zhang, S., et al. (2018). Self-consistent determination of spin Hall angle and spin diffusion length in Pt and Pd: the role of the interface spin loss. Sci. Adv. *4*, eaat1670.

Torrejon, J., Riou, M., Araujo, F.A., Tsunegi, S., Khalsa, G., Querlioz, D., Bortolotti, P., Cros, V., Yakushiji, K., Fukushima, A., et al. (2017). Neuromorphic computing with nanoscale spintronic oscillators. Nature *547*, 428–431.

Tsai, H., Higo, T., Kondou, K., Nomoto, T., Sakai, A., Kobayashi, A., Nakano, T., Yakushiji, K., Arita, R., Miwa, S., et al. (2020). Electrical manipulation of a topological antiferromagnetic state. Nature *580*, 608–613.

Tshitoyan, V., Ciccarelli, C., Mihai, A., Ali, M., Irvine, A., Moore, T., Jungwirth, T., and Ferguson, A. (2015). Electrical manipulation of ferromagnetic NiFe by antiferromagnetic IrMn. Phys. Rev. B *92*, 214406.

Tu, S., Ziman, T., Yu, G., Wan, C., Hu, J., Wu, H., Wang, H., Liu, M., Liu, C., and Guo, C. (2020). Record thermopower found in an IrMn-based spintronic stack. Nat. Commun. *11*, 2023.

Vincent, A.F., Larroque, J., Locatelli, N., Romdhane, N.B., Bichler, O., Gamrat, C., Zhao, W.S., Klein, J.-O., Galdin-Retailleau, S., and Querlioz, D. (2015). Spin-transfer torque magnetic memory as a stochastic memristive synapse for neuromorphic systems. IEEE Trans. Biomed. circuits Syst. *9*, 166–174.

Vlaminck, V., Pearson, J.E., Bader, S.D., and Hoffmann, A. (2013). Dependence of spin-pumping spin Hall effect measurements on layer thicknesses and stacking order. Phys. Rev. B *88*, 064414.

Wadley, P., Howells, B., Železný, J., Andrews, C., Hills, V., Campion, R.P., Novák, V., Olejník, K., Maccherozzi, F., Dhesi, S.S., et al. (2016). Electrical switching of an antiferromagnet. Science *351*, 587.

Walter, M., Walowski, J., Zbarsky, V., Münzenberg, M., Schäfers, M., Ebke, D., Reiss, G., Thomas, A., Peretzki, P., and Seibt, M. (2011). Seebeck effect in magnetic tunnel junctions. Nat. Mater. *10*, 742–746.

Wan, C., Zhang, X., Yuan, Z., Fang, C., Kong, W., Zhang, Q., Wu, H., Khan, U., and Han, X. (2017). Programmable spin logic based on spin Hall effect in a single device. Adv. Electron. Mater. *3*, 1600282.

Wang, H., Du, C., Pu, Y., Adur, R., Hammel, P.C., and Yang, F. (2014). Scaling of spin Hall angle in 3d, 4d, and 5d metals from $Y_3Fe_5O_{12}$/metal spin pumping. Phys. Rev. Lett. *112*, 197201.

Wang, K. (2018). Complementary logic with a spin. Nat. Electron. *1*, 378–379.

Wang, M., Cai, W., Zhu, D., Wang, Z., Kan, J., Zhao, Z., Cao, K., Wang, Z., Zhang, Y., Zhang, T., et al. (2018a). Field-free switching of a perpendicular magnetic tunnel junction through the interplay of spin–orbit and spin-transfer torques. Nat. Electron. *1*, 582–588.

Wang, W.-G., Li, M., Hageman, S., and Chien, C. (2012). Electric-field-assisted switching in magnetic tunnel junctions. Nat. Mater. *11*, 64–68.

Wang, X., Tang, J., Xia, X., He, C., Zhang, J., Liu, Y., Wan, C., Fang, C., Guo, C., Yang, W., et al. (2019a). Current-driven magnetization switching in a van der Waals ferromagnet Fe_3GeTe_2. Sci. Adv. *5*, eaaw8904.

Wang, X., Wan, C., Kong, W., Zhang, X., Xing, Y., Fang, C., Tao, B., Yang, W., Huang, L., Wu, H., et al. (2018b). Field-free programmable spin logics via chirality-reversible spin–orbit torque switching. Adv. Mater. *30*, 1801318.

Wang, Y., Zhu, D., Wu, Y., Yang, Y., Yu, J., Ramaswamy, R., Mishra, R., Shi, S., Elyasi, M., Teo, K.-L., et al. (2017). Room temperature magnetization switching in topological insulator-ferromagnet heterostructures by spin-orbit torques. Nat. Commun. *8*, 1364.

Wang, Y., Zhu, D.P., Yang, Y.M., Lee, K., Mishra, R., Go, G., Oh, S.H., Kim, D.H., Cai, K.M., Liu, E.L., et al. (2019b). Magnetization switching by magnon-mediated spin torque through an antiferromagnetic insulator. Science *366*, 1125–1128.

Wang, Z., Joshi, S., Savel'ev, S., Song, W., Midya, R., Li, Y., Rao, M., Yan, P., Asapu, S., Zhuo, Y., et al. (2018c). Fully memristive neural networks for pattern classification with unsupervised learning. Nat. Electron. *1*, 137–145.

Wang, Z., Zhang, L., Wang, M., Wang, Z., Zhu, D., Zhang, Y., and Zhao, W. (2018d). High-density NAND-like spin transfer torque memory with spin orbit torque erase operation. IEEE Electron. Device Lett. *39*, 343–346.

Wu, H., Nance, J., Razavi, S.A., Lujan, D., Dai, B., Liu, Y., He, H., Cui, B., Wu, D., and Wong, K. (2020a). Chiral symmetry breaking for deterministic switching of perpendicular magnetization by spin-orbit torque. arXiv. arXiv:2004.13872.

Wu, K., Su, D., Saha, R., and Wang, J.-P. (2020b). Deterministic field-free switching of a perpendicularly magnetized ferromagnetic layer via the joint effects of the Dzyaloshinskii–Moriya interaction and damping-and field-like spin–orbit torques: an appraisal. J. Phys. D Appl. Phys. *53*, 205002.

Wu, Y., Elyasi, M., Qiu, X., Chen, M., Liu, Y., Ke, L., and Yang, H. (2017). High-performance THz emitters based on ferromagnetic/nonmagnetic heterostructures. Adv. Mater. *29*, 1603031.

Xia, Q., and Yang, J.J. (2019). Memristive crossbar arrays for brain-inspired computing. Nat. Mater. *18*, 309–323.

Xie, Q., Lin, W., Yang, B., Shu, X., Chen, S., Liu, L., Yu, X., Breese, M.B., Zhou, T., Yang, M., et al. (2019). Giant enhancements of perpendicular magnetic anisotropy and spin-orbit torque by a MoS_2 layer. Adv. Mater. *31*, 1900776.

Xu, H., Wei, J., Zhou, H., Feng, J., Xu, T., Du, H., He, C., Huang, Y., Zhang, J., Liu, Y., et al. (2020). High spin Hall conductivity in large-area type-II Dirac semimetal $PtTe_2$. Adv. Mater. *32*, e2000513.

Yang, M., Cai, K., Ju, H., Edmonds, K.W., Yang, G., Liu, S., Li, B., Zhang, B., Sheng, Y., Wang, S., et al. (2016). Spin-orbit torque in Pt/CoNiCo/Pt symmetric devices. Sci. Rep. *6*, 20778.

Yang, M., Deng, Y., Cai, K., Ju, H., Liu, S., Li, B., and Wang, K. (2019a). Deterministic magnetic switching of perpendicular magnets by gradient current density. J. Magn. Magn. Mater. *489*, 165474.

Yang, M., Deng, Y., Wu, Z., Cai, K., Edmonds, K.W., Li, Y., Sheng, Y., Wang, S., Cui, Y., Luo, J., et al. (2019b). Spin logic devices via electric field controlled magnetization reversal by spin-orbit torque. IEEE Electron. Device Lett. *40*, 1554–1557.

Yang, S.-H., Garg, C., Phung, T., Rettner, C., and Hughes, B. (2019c). Spin-orbit torque driven one-bit magnetic racetrack devices-memory and neuromorphic applications. In 2019 International Symposium on VLSI Technology, Systems and Application (VLSI-TSA) (IEEE). https://doi.org/10.1109/VLSI-TSA.2019.8804677.

You, L., Lee, O., Bhowmik, D., Labanowski, D., Hong, J., Bokor, J., and Salahuddin, S. (2015). Switching of perpendicularly polarized nanomagnets with spin orbit torque without an external magnetic field by engineering a tilted anisotropy. Proc. Natl. Acad. Sci.U S A *112*, 10310–10315.

Yu, G., Upadhyaya, P., Fan, Y., Alzate, J.G., Jiang, W., Wong, K.L., Takei, S., Bender, S.A., Chang, L.-T., Jiang, Y., et al. (2014). Switching of perpendicular magnetization by spin–orbit torques in the absence of external magnetic fields. Nat. Nanotechnology *9*, 548–554.

Yu, G., Upadhyaya, P., Li, X., Li, W., Kim, S.K., Fan, Y., Wong, K.L., Tserkovnyak, Y., Amiri, P.K., and Wang, K.L. (2016). Room-temperature creation and spin–orbit torque manipulation of skyrmions in thin films with engineered asymmetry. Nano Lett. *16*, 1981–1988.

Yu, J., Bang, D., Mishra, R., Ramaswamy, R., Oh, J.H., Park, H.-J., Jeong, Y., Van Thach, P., Lee, D.-K., Go, G., et al. (2019). Long spin coherence length and bulk-like spin–orbit torque in ferrimagnetic multilayers. Nat. Mater. *18*, 29–34.

Yu, Z., Zhang, Y., Zhang, Z., Cheng, M., Lu, Z., Yang, X., Shi, J., and Xiong, R. (2018). Domain-wall motion at an ultrahigh speed driven by spin–orbit torque in synthetic antiferromagnets. Nanotechnology *29*, 175404.

Yue, K., Liu, Y., Lake, R.K., and Parker, A.C. (2019). A brain-plausible neuromorphic on-the-fly learning system implemented with magnetic domain wall analog memristors. Sci. Adv. *5*, eaau8170.

Yun, J., Bai, Q., Yan, Z., Chang, M., Mao, J., Zuo, Y., Yang, D., Xi, L., and Xue, D. (2020). Tailoring multilevel-stable remanence states in exchange-biased system through spin-orbit torque. Adv. Funct. Mater. *30*, 1909092.

Zahedinejad, M., Awad, A.A., Muralidhar, S., Khymyn, R., Fulara, H., Mazraati, H., Dvornik, M., and Akerman, J. (2020). Two-dimensional mutually synchronized spin Hall nano-oscillator arrays for neuromorphic computing. Nat. Nanotechnol. *15*, 47–52.

Železný, J., Gao, H., Výborný, K., Zemen, J., Mašek, J., Manchon, A., Wunderlich, J., Sinova, J., and Jungwirth, T. (2014). Relativistic néel-order fields induced by electrical current in antiferromagnets. Phys. Rev. Lett. *113*, 157201.

Zhang, C., Fukami, S., Watanabe, K., Ohkawara, A., Duttagupta, S., Sato, H., Matsukura, F., and Ohno, H. (2016a). Critical role of W deposition condition on spin-orbit torque induced magnetization switching in nanoscale W/CoFeB/MgO. Appl. Phys. Lett. *109*, 192405.

Zhang, N., Cao, Y., Li, Y., Rushforth, A.W., Ji, Y., Zheng, H., and Wang, K. (2020a). Complementary lateral-spin-orbit building blocks for programmable logic and in-memory computing. Adv. Electron. Mater. *6*, 2000296.

Zhang, N., Zhang, B., Yang, M., Cai, K., Sheng, Y., Li, Y., Deng, Y., and Wang, K. (2017). Progress of electrical control magnetization reversal and domain wall motion. Acta Phys. Sin. *66*, 027501.

Zhang, P., Finley, J., Safi, T., and Liu, L. (2019a). Quantitative study on current-induced effect in an antiferromagnet insulator/Pt bilayer film. Phys. Rev. Lett. *123*, 247206.

Zhang, P., Liao, L., Shi, G., Zhang, R., Wu, H., Wang, Y., Pan, F., and Song, C. (2018). Spin-orbit torque in a completely compensated synthetic antiferromagnet. Phys. Rev. B *97*, 214403.

Zhang, R., Liao, L., Chen, X., Xu, T., Cai, L., Guo, M., Bai, H., Sun, L., Xue, F., and Su, J. (2020b). Current-induced magnetization switching in a CoTb amorphous single layer. Phys. Rev. B *101*, 214418.

Zhang, S., Luo, S., Xu, N., Zou, Q., Song, M., Yun, J., Luo, Q., Guo, Z., Li, R., and Tian, W. (2019b). A spin–orbit-torque memristive device. Adv. Electron. Mater. *5*, 1800782.

Zhang, W., Han, W., Jiang, X., Yang, S.-H., and Parkin, S. (2015). Role of transparency of platinum–ferromagnet interfaces in determining the intrinsic magnitude of the spin Hall effect. Nat. Phys. *11*, 496–502.

Zhang, W., Han, W., Yang, S.-H., Sun, Y., Zhang, Y., Yan, B., and Parkin, S.S. (2016b). Giant facet-dependent spin-orbit torque and spin Hall conductivity in the triangular antiferromagnet $IrMn_3$. Sci. Adv. *2*, e1600759.

Zhang, W., Jungfleisch, M.B., Jiang, W., Pearson, J.E., Hoffmann, A., Freimuth, F., and Mokrousov, Y. (2014). Spin Hall effects in metallic antiferromagnets. Phys. Rev. Lett. *113*, 196602.

Zhao, B., Khokhriakov, D., Zhang, Y., Fu, H., Karpiak, B., Hoque, A.M., Xu, X., Jiang, Y., Yan, B., and Dash, S.P. (2020). Observation of charge to spin conversion in Weyl semimetal WTe_2 at room temperature. Phys. Rev. Res. *2*, 013286.

Zhou, Z.P., Liu, X.H., and Wang, K.Y. (2020). Controlling vertical magnetization shift by spin–orbit torque in ferromagnetic/antiferromagnetic/ferromagnetic heterostructure. Appl. Phys. Lett. *116*, 062403.

Zhu, L., Ralph, D., and Buhrman, R. (2019a). Spin-orbit torques in heavy-metal–ferromagnet bilayers with varying strengths of interfacial spin-orbit coupling. Phys. Rev. Lett. *122*, 077201.

Zhu, L., Ralph, D.C., and Buhrman, R.A. (2018). Highly efficient spin-current generation by the spin Hall effect in $Au_{1-x}Pt_x$. Phys. Rev. Appl. *10*, 031001.

Zhu, L., Zhu, L., Shi, S., Sui, M., Ralph, D., and Buhrman, R. (2019b). Enhancing spin-orbit torque by strong interfacial scattering from ultrathin insertion layers. Phys. Rev. Appl. *11*, 061004.

Zhu, L., Zhu, L., Sui, M., Ralph, D.C., and Buhrman, R.A. (2019c). Variation of the giant intrinsic spin Hall conductivity of Pt with carrier lifetime. Sci. Adv. *5*, eaav8025.

Zidan, M.A., Strachan, J.P., and Lu, W.D. (2018). The future of electronics based on memristive systems. Nat. Electron. *1*, 22–29.